

**A machine learning approach targeting parameter estimation for plant functional type coexistence modeling using ELM-FATES (v2.0)**

Lingcheng Li<sup>1</sup>, Yilin Fang<sup>2</sup>, Zhonghua Zheng<sup>3</sup>, Mingjie Shi<sup>1</sup>, Marcos Longo<sup>4</sup>, Charles D. Koven<sup>4</sup>, Jennifer A. Holm<sup>4</sup>, Rosie A. Fisher<sup>5</sup>, Nate G. McDowell<sup>1,6</sup>, Jeffrey Chambers<sup>4</sup>, L. Ruby Leung<sup>1</sup>

1. Atmospheric Sciences and Global Change Division, Pacific Northwest National Laboratory, Richland, WA, USA

2. Earth System and Science Division, Pacific Northwest National Laboratory, Richland, WA, USA

3. Department of Earth and Environmental Sciences, The University of Manchester, Manchester, UK

4. Climate and Ecosystem Sciences Division, Lawrence Berkeley National Laboratory, Berkeley, CA, USA

5. CICERO Center for International Climate and Environmental Research, Oslo, Norway

6. School of Biological Sciences, Washington State University, PO Box 644236, Pullman, WA, USA

Correspondence to: Lingcheng Li ([lingcheng.li@pnnl.gov](mailto:lingcheng.li@pnnl.gov))

## Abstract

Tropical forest dynamics play a crucial role in the global carbon, water, and energy cycles. However, realistically simulating the dynamics of competition and coexistence between different plant functional types (PFTs) in tropical forests remains a significant challenge. This study aims to improve the modeling of PFT coexistence in the Functionally Assembled Terrestrial Ecosystem Simulator (FATES), a vegetation demography model implemented in the Energy Exascale Earth System Model (E3SM) land model (ELM), ELM-FATES. Specifically, we explore (1) whether plant trait relationships established from field measurements can constrain ELM-FATES simulations; and (2) whether machine learning (ML) based surrogate models can emulate the complex ELM-FATES model and optimize parameter selections to improve PFT coexistence modeling. We conducted three ensembles of ELM-FATES experiments at a tropical forest site near Manaus, Brazil. By comparing the ensemble experiments without (Exp-CTR) and with (Exp-OBS) consideration of observed trait relationships, we found that accounting for these relationships slightly improves the simulations of water, energy, and carbon variables when compared to observations, but degrades the simulation of PFT coexistence. Using ML based surrogate models trained on Exp-CTR, we optimized the trait parameters in ELM-FATES, and conducted another ensemble of experiments (Exp-ML) with these optimized parameters. The proportion of PFT coexistence experiments significantly increased from 21% in Exp-CTR to 73% in Exp-ML. After filtering the experiments that allow for PFT coexistence to agree with observations (within 15% tolerance), 33% of the Exp-ML experiments were retained, which is a significant improvement compared to the 1.4% in Exp-CTR. Exp-ML also well reproduces the annual means and seasonal variations of water, energy and carbon fluxes, and the field inventory of above ground biomass. This study represents a reproducible method, which utilizes machine learning to identify parameter values that improve model fidelity against observations and PFT coexistence in vegetation demography models for diverse ecosystems. Our study also suggests the need for new mechanisms to enhance the robust simulation of coexisting plants in ELM-FATES, and has significant implications for modeling the response and feedbacks of ecosystem dynamics to climate change.

## 1. Introduction

Tropical ecosystems feature the highest biodiversity on Earth, maintaining more than 75% of all known species (Mora et al., 2011; Mitchard, 2018). The dynamics of tropical forests are closely related to the regional and global carbon, energy and water cycles (Bonan, 2008; Piao et al., 2020). Vegetation is expected to face more water stress from vapor pressure deficit increase and soil moisture reduction with global warming (McDowell et al., 2020). Tree mortality rates are accelerating in some tropical regions due to rising atmospheric water stress (Bauman et al., 2022; Hubau et al., 2020; Zuleta et al., 2017). Tropical forests currently make an approximately neutral contribution to the global carbon cycle as a result of a large land-use source balanced by sinks in recovering and undisturbed forests, but they may become a carbon source in the future under the threat of climate change and human-induced disturbance (Mitchard, 2018; Gatti et al., 2021). Therefore, understanding and modeling tropical forest dynamics and related feedbacks have crucial implications for projecting future changes in the global climate system.

Dynamic global vegetation models (DGVMs) are the primary tools to simulate terrestrial ecosystem dynamics of plant functional type distribution, ecosystem composition and functioning, and ecosystem response to and recovery from disturbance (e.g., fire and wind damage) (Longo et al., 2019; Fisher et al., 2018; Foley et al., 1996; Sitch et al., 2003; Cao and Woodward, 1998; Berzaghi et al., 2019; McMahon et al., 2011). Conventional DGVMs represent plant communities using an area-averaged representation of plant functional types (PFTs) in each grid cell. Their relatively simple structures have the advantage of high computational efficiency for use in Earth system models (Fisher et al., 2018; Snell et al., 2014). However, these models do not capture many demographic processes. For example, plants of each represented PFT typically have identical

properties (e.g., tree size), which limits the capability of modeling ecosystem dynamics and functioning of canopy gap formation, PFT competition, and disturbance reactions (Feeley et al., 2007; Stark et al., 2012; Hurtt et al., 1998; Moorcroft, 2003; Brister et al., 2020). To address these limitations, researchers have developed new generation DGVMs called vegetation demographic models (VDMs), commonly including individual-based models and cohort-based models (Fisher et al., 2018). The individual-based models, also known as forest gap models, explicitly represent vegetation as individual plants and simulate their birth, growth, and death (Fyllas et al., 2014; Christoffersen et al., 2016; Sato et al., 2007; Jonard et al., 2020; Maréchaux and Chave, 2017). These models incorporate the stochasticity and heterogeneity of the plant light environment mechanistically and thereby can typically represent PFT competitive exclusion, succession, and coexistence. However, explicit simulations of individual plants with stochastic processes suffer a substantial computational penalty and limit applicability over large or global scales (Fisher et al., 2018). To capture sufficient ecosystem dynamics and maintain relatively high computational efficiency, "cohort-based" models have been proposed (Haverd et al., 2013; Medvigy et al., 2009; Ma et al., 2021; Moorcroft et al., 2001; Weng et al., 2015; Longo et al., 2019; Belda et al., 2022). In cohort-based approaches, individual plants are grouped together as "cohorts" based on their similar properties, including size, age, and PFT (Fisher et al., 2018). Many cohort-based models have been developed and widely used across regional to global scales. Examples of cohort-based models include the Ecosystem Demography model (ED) (Moorcroft et al., 2001), the Functionally Assembled Terrestrial Ecosystem Simulator (FATES) (Fisher et al., 2018, 2015), and the Geophysical Fluid Dynamics Laboratory (GFDL) Land Model 3 with the Perfect Plasticity Approximation (LM3-PPA) (Weng et al., 2015). In this study, we employ the FATES model, a widely used tool for modeling ecosystem dynamics in multiple ecosystems, including tropical



(Holm et al., 2020; Koven et al., 2020; Chitra-Tarak et al., 2021; Cheng et al., 2021), boreal (Lambert et al. 2022) and mixed-conifer forests (Buotte et al., 2021), and forest disturbance (Huang et al., 2020).

Despite ongoing applications, robust simulations of competition and coexistence in cohort-based VDMs remain a major challenge. In niche-based coexistence theory, coexisting species require both convergence in strategy to adapt to the surrounding environment ("environmental filtering") and divergence in strategy to ensure differentiation in resource requirements ("niche partitioning") (Kraft et al., 2008; Adler et al., 2013). These same constraints apply to coexisting PFTs as modeled by VDMs. Thus, on the one hand, VDMs need to include mechanisms that capture critical niche dimensions (e.g., spatial and temporal variation in light, water, and nutrients). For example, the multi-layer canopy structure in FATES provides vertical light resource differentiation. Another essential aspect is to assign reasonable plant functional traits (i.e., the parameters that define a given plant functional type) to satisfy environmental filtering, ensure niche partitioning, and consequently preserve PFT coexistence. Considering the relatively high computational cost of VDMs and the host land surface models, it is not feasible to directly apply global optimization methods such as Shuffled Complex Evolution (Duan et al., 1992) to calibrate trait-related parameters, because this could be time-consuming and computationally intensive (Rouholahnejad et al., 2012). Therefore, most previous studies use the filtered ensemble approach to select trait-related parameters involving several steps: 1) generate a parameter ensemble based on reference trait ranges or correlations, 2) conduct ensemble model simulations, and 3) filter the parameter ensemble by coexistence and other criteria (e.g., observation constraints). For example, Huang et al. (2020) applied FATES implemented in the Community Land Model (CLM; herein CLM-

FATES) with two tropical PFTs to study forest dynamics at tropical sites. They performed 70 one-at-a-time experiments before obtaining one reasonable parameter set. Buottte et al. (2021) used CLM-FATES to simulate forest dynamics of pine and incense cedar over the Sierra Nevada of California, and their two stages of experiments (360 plus 72 runs) only yielded four sets of parameters that met the given criteria. The filtered ensemble approach has low efficiency, which hinders VDMs' application to modeling ecosystem dynamics under the changing climate. In addition, trait relationships derived from field measurements are often used to infer parameter selections when simulating coexistence. For example, Longo et al. (2020) used multiple trait relationships derived from various datasets to guide parameter selection for different PFTs in the ED-2.2 model simulations. However, whether the observed trait relationships can efficiently improve PFT coexistence simulation in current VDMs is still unclear. Earlier studies using FATES have also highlighted the importance of reproductive feedbacks in maintaining or prohibiting coexistence (Fisher et al. 2010; Maréchaux and Chave 2017). But fundamentally, if PFTs have highly contrasting reproductive output, the model tends towards competitive exclusion, so discerning areas with at least approximately equal fitness is necessary. While representing a large number of plant functional types may improve the likelihood of coexistence (Koven et al., 2020), this comes at a considerable computational expense.

Machine learning (ML) has facilitated Earth science studies (Shen, 2018; Nearing et al., 2021; Zhu et al., 2022; Pal et al., 2019; Jung et al., 2019), possibly providing a promising approach to improve PFT coexistence modeling in VDMs. ML algorithms have been broadly and successfully employed in recent decades. They can be used as standalone models to predict variables of interest or integrated with process-based models to improve simulations (Xu and Liang, 2021; He et al.,

2022; Peatier et al., 2022). Among these applications, ML has shown advantages as a surrogate model for parameter optimization and sensitivity quantification, including its effectiveness and easy application, its ability to implicitly deal with complex nonlinear correlations and high dimensional data, and handle interactions between variables (Sit et al., 2020; Antoniadis et al., 2020; Tsai et al., 2021). One promising approach is to construct ML-based surrogate models using data from initial model simulations to emulate the relationship between inputs (i.e., model parameters) and model outputs (Wang et al., 2014). Then the computationally inexpensive surrogate model can be efficiently used for parameter optimization and sensitivity analysis. For example, Dagon et al. (2020) implemented artificial neural networks to emulate the satellite leaf area constrained version of CLM5 (Lawrence et al., 2019) and estimated optimal parameters to improve the global simulation of gross primary production and latent heat flux. Sawada (2020) developed an ML surrogate model to optimize the land surface model parameters and improve soil moisture and vegetation dynamics simulations. Watson-Parris et al. (2021) built a general tool to efficiently emulate Earth system models for uncertainty quantification and model calibration. Although employing ML based surrogate models to optimize the trait parameters and hence improve the vegetation dynamics modeling in VDMs is promising, this area of research remains under-explored.

This study aims to improve PFT coexistence modeling in VDMs. The cohort-based FATES implemented in the Energy Exascale Earth System Model (E3SM) land model (ELM; Golaz et al., 2019), i.e., ELM-FATES, is taken as our testbed. The ELM land model simulates surface energy fluxes, soil and canopy biophysics, hydrology, and soil biogeochemistry, whereas FATES simulates live vegetation processes, litter dynamics, and fire. We first examine whether trait

161 relationships constructed from field measurements can help improve ELM-FATES simulations.  
162 Second, we explore whether ML based surrogate models can help optimize key trait parameters in  
163 ELM-FATES to improve the simulation of PFTs coexistence. Our model experiments are  
164 conducted for a tropical rainforest site located in Manaus, Brazil. This paper is organized as  
165 follows. Section 2 describes ELM-FATES, summarizes the key functional trait-related parameters,  
166 introduces the machine learning algorithms, and explains the overall experimental design. Results  
167 are presented in Section 3, followed by Discussions and Conclusions in Section 4 and Section 5,  
168 respectively.

## **2. Methodology**

### **2.1 Study site and data**

Our study site is located at kilometer 34 (K34) of the ZF2 road, Manaus, Brazil (latitude: -2.6091 S; longitude: -60.2093 W). The K34 site is an old-growth primary forest with minimal human disturbances (Holm et al., 2020). The annual precipitation is about 2252 mm, and the mean temperature is about 26.68 °C (<https://ameriflux.lbl.gov/sites/siteinfo/BR-Ma2>). The wet season is from November to May, and the dry season is from June to October (Fang et al., 2017). Hourly meteorological forcing (i.e., precipitation, air temperature, relative humidity, wind speed, surface pressure) at the K34 eddy covariance flux tower from 2002–2005 was obtained from the LBA-ECO CD-32 Flux Tower Network Data Compilation (Restrepo-Coupe et al., 2021). Observational reference datasets obtained from Holm et al. (2020) include gross primary production (GPP), evapotranspiration (ET), sensible heat flux (SH), Bowen ratio (BW, the ratio between sensible heat and latent heat), and inventory data-based aboveground biomass (AGB). The GPP, ET, SH, and BW observations are monthly climatological averages from 2000 to 2008 (Table S1). The AGB at this site is about  $303 \pm 2.3$  Mg/ha. These observational data were used to evaluate the ELM-FATES simulations and constrain the ML surrogate models.

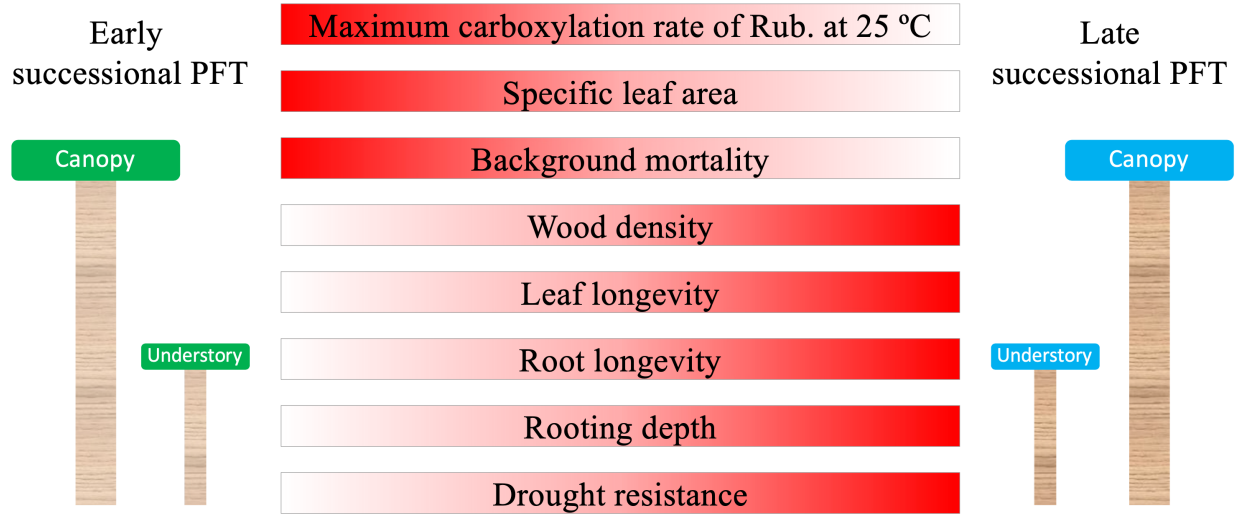
### **2.2 ELM-FATES and parameters**

ELM-FATES is used as the model testbed. ELM is the land model of E3SM, which is the host land model of FATES (Golaz et al., 2019; Leung et al., 2020; Holm et al., 2020). FATES is a size- and age-structured vegetation model developed from the Community Land Model with ecosystem demography (CLM-ED) (Fisher et al., 2015; Koven et al., 2020). FATES includes two key structural components: ecosystem demography (ED; Moorcroft et al., 2001) and a modified

version of perfect plasticity approximation (PPA, Purves et al., 2008). FATES discretizes the simulated landscape into spatially implicit "*patches*" representing different disturbance histories of the ecosystem since the last disturbance. Within each patch, the hypothetical population of plants is grouped into "*cohorts*": a cohort consists of a population density of trees with similar size and the same plant functional type. Cohorts are organized, via the PPA concept, into canopy layers, and compete for light based on their canopy vertical positions (e.g., canopy layer vs. understory layer). The understory layer is formed when the canopy area becomes greater than the total ground area, and some fraction of each cohort is 'demoted' to the understory as a function of its height. The number of patches and cohorts varies depending on processes, including recruitment, growth, mortality, competition, and disturbance. The modified PPA probabilistically splits cohorts into discrete canopy and understory layers based on a function of their height (Strigul et al., 2008; Fisher et al., 2010). A detailed description of the FATES model can be found in its technical note (Zenodo, <https://doi.org/10.5281/zenodo.3517272>).

In this study, we configured two PFTs in ELM-FATES, i.e., early successional and late successional broadleaf evergreen tropical trees, which can represent a primary axis of variability in tropical forests (Huang et al., 2020; Reich, 2014; Díaz et al., 2016). There are tradeoffs between the plant traits of these two PFTs. Compared with the late successional PFT, the early successional PFT is more light-demanding and fast-growing, but with lower woody density, shorter leaf and root lifespans, and higher background mortality. To represent the drought impacts on forest dynamics, the early successional PFT is further assumed to be less drought resistant with shallower rooting depth and hence more easily affected by drought conditions (Oliveira et al., 2021). The corresponding tradeoffs and parameters between these two PFTs are shown in Figure 1 and Table

215 1.



216

217 Figure 1. Schematic representation of tradeoffs between early and late successional PFTs. Dark  
 218 red denotes a higher parameter value. The tradeoffs of the top five traits are used to constrain the  
 219 parameter sampling.

220

Table 1 Summary of ELM-FATES trait parameters for two PFTs

Parameter type	Parameter name	Symbol	Unit	Early PFT	Late PFT	Range
Optimized parameter	Maximum carboxylation rate of Rub. at 25 °C, canopy top	$V_{cmax}$	$\mu\text{mol CO}_2/\text{m}^2/\text{s}$	$V_{cmax,early} > V_{cmax,late}$		40–105
	Specific leaf area, canopy top	$SLA$	$\text{m}^2/\text{gC}$	$SLA_{early} > SLA_{late}$		0.005–0.04
	Background mortality rate	$M_{bk}$	1/yr	$M_{bk,early} > M_{bk,late}$		0.005–0.05
	Wood density	$WD$	$\text{g}/\text{cm}^3$	$WD_{early} < WD_{late}$		0.2–1.0
	Leaf longevity	$L_{leaf}$	year	$L_{leaf,early} < L_{leaf,late}$		0.2–3.0
Fixed parameter	Maximum size of storage C pool, relative to the maximum size of leaf C pool	$CR_{s2l}$	—	same		0.8–1.5
	Root longevity	$L_{root}$	year	0.9	2.6	—
	Fine rooting distribution profile parameter a	$R_a$	—	7	7	—
	Fine rooting distribution profile parameter b	$R_b$	—	2	0.4	—
	BTRAN threshold below which drought mortality begins.	$M_{btran}$	—	0.4	1.0E-06	—
	Soil water potential at full stomatal closure	$\psi_{closure}$	mm	–113000	–242000	—

221

222

223

224

225

\*Parameter references (Huang et al., 2020; Koven et al., 2020; Longo et al., 2020; Holm et al., 2020; Cheng et al., 2021; Domingues et al., 2005; Chitra-Tarak et al., 2021; Buotte et al., 2021)

\* $R_a$  and  $R_b$  are parameters that determine the rooting depth and vertical distribution of fine roots.

\*BTRAN is the plant water stress factor. BTRAN  $\in [0,1]$ , 0 representing full water stress, 1 representing no water stress.

### 2.3 Machine learning algorithm

We built ML-based surrogate models to emulate ELM-FATES simulations. To represent the relationships between ELM-FATES parameters and simulations (e.g., AGB), we used eXtreme Gradient Boosting (XGBoost; Chen and Guestrin, 2016), a decision-tree-based ensemble machine learning algorithm. Ensemble learning techniques combine the predictions of multiple independent base models (e.g., decision trees) to produce more accurate predictions, with popular algorithms such as Random Forest (Breiman, 2001) and XGBoost. While Random Forest builds an ensemble of parallel trees using bagging and produces the final prediction by averaging the outputs of all individual trees, XGBoost sequentially trains a set of decision trees using boosting (Friedman, 2001), where each successive tree corrects the mistakes of its predecessors, and the final prediction is obtained by combining the predictions of all trees using a weighted sum. XGBoost not only handles complex nonlinear interactions and collinearity between different features, but also provides a parallel implementation that effectively solves a range of data science problems. It has been successfully applied in a variety of fields within Earth and Environmental Sciences, such as urban temperature emulation (Zheng et al., 2021b), wildfire burned area (Wang et al., 2021), and emissions prediction (Wang et al., 2022), flash flood risk assessment (Ma et al., 2021), and aerosol property estimation (Zheng et al., 2021a, c).

### 2.4 Experimental design

The experimental design flowchart is shown in Figure 2. Overall, we generated three ensembles of parameter values, i.e., Par-CTR, Par-OBS, and Par-ML, and conducted three ensembles of corresponding ELM-FATES experiments, i.e., Exp-CTR, Exp-OBS, and Exp-ML. Exp-CTR is the control experiment without being constrained by the observed trait relationships. Exp-OBS



considered the constraint of the observed trait relationships. The Par-ML was generated by machine learning surrogate models, which were trained based on Exp-CTR, and then used to conduct Exp-ML. The detailed experiment procedures are described below.

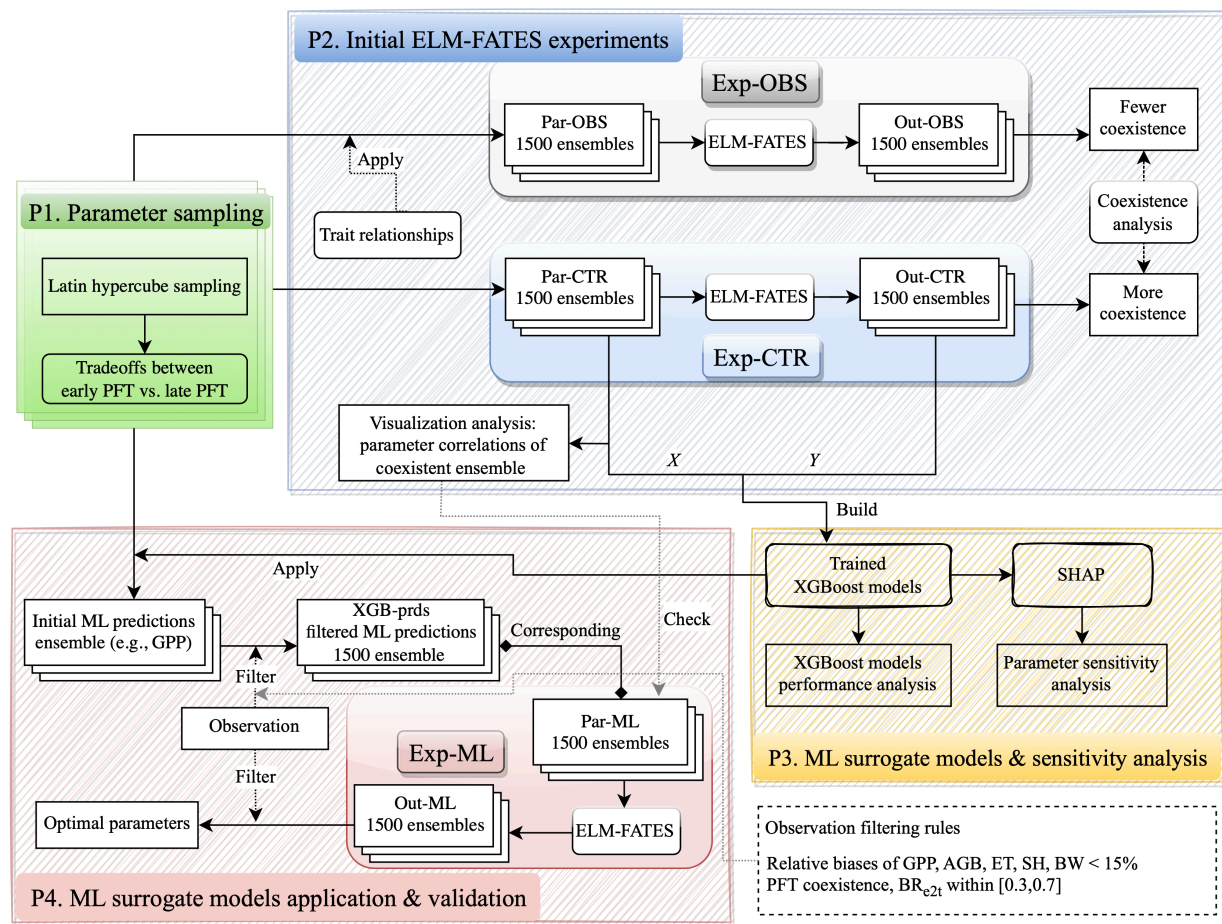


Figure 2. Overall flowchart of experimental design and associated analysis.

#### 2.4.1 Procedure 1: Parameter sampling

The procedure "P1" in Fig. 2 is used to generate an ensemble of parameter values for each experiment ensemble, i.e., Exp-CTR, Exp-OBS, and Exp-ML. First, a number of initial parameter sets (e.g., 5000 sets) were generated using Latin Hypercube Sampling (LHS; Mckay et al., 2000). Second, the initial parameter sets were filtered by the trait tradeoffs between early and late successional PFTs (Figure 1). We repeatedly increased the number of initial parameter sets in the first step until 1500 parameter sets were obtained in the second step. Each ELM-FATES experiment starts from bare ground and runs for 350 years to reach an equilibrium state, by cycling the meteorological forcing during 2002–2005, and the last four years of the simulations were analyzed.

#### 2.4.2 Procedure 2: Initial ELM-FATES experiments of Exp-CTR and Exp-OBS

To test whether plant trait relationships established from field measurements can improve the ELM-FATES simulations, we derived three trait relationships based on the tropical studies of Koven et al. (2020) and Longo et al. (2020). Using the digitized data from Figure 3 in Koven et al. (2020), the background mortality  $M_{bk}$  (see table 1 for parameter definitions) can be empirically computed from the maximum carboxylation rate  $V_{cmax}$ ,

$$M_{bk} = 0.0082 \times e^{(0.0153 \times V_{cmax})} \quad (1)$$

Based on the equations in Figure S18 of Longo et al. (2020), the leaf longevity  $L_{leaf}$  and wood density  $WD$  can be calculated via the specific leaf area  $SLA$ ,

$$L_{leaf} = 0.0001 \times SLA^{(-2.32)} \quad (2)$$

$$WD = -0.583 \times \ln(SLA) - 1.6754 \quad (3)$$

These trait relationships were used to generate parameters for Par-OBS.

Two initial sets of experiment ensembles, i.e., Exp-CTR and Exp-OBS (procedure "P2" in Figure 2), were conducted based on Par-CTR and Par-OBS, respectively. For Par-CTR, 1500 parameter sets were generated from the procedure "P1" based on the entire eleven parameters' space, i.e.,  $V_{cmax,early}$ ,  $V_{cmax,late}$ ,  $SLA_{early}$ ,  $SLA_{late}$ ,  $M_{bk,early}$ ,  $M_{bk,late}$ ,  $WD_{early}$ ,  $WD_{late}$ ,  $L_{leaf,early}$ ,  $L_{leaf,late}$ ,  $CR_{s2l}$  (maximum size of storage C pool relative to the maximum size of leaf C pool, Table 1). For Par-OBS, 1500 parameter sets were generated from the procedure "P1" but only based on five parameters' space (i.e.,  $V_{cmax,early}$ ,  $V_{cmax,late}$ ,  $SLA_{early}$ ,  $SLA_{late}$ ,  $CR_{s2l}$ ). The other six parameters ( $M_{bk,early}$ ,  $M_{bk,late}$ ,  $WD_{early}$ ,  $WD_{late}$ ,  $L_{leaf,early}$ ,  $L_{leaf,late}$ ) in Par-OBS were calculated based on the traits relationships defined by Equations (1) ~ (3). Therefore, compared to Par-CTR, the parameters in Par-OBS are constrained by the observed trait relationships. The distributions of these two parameter sets are shown in Figure S1.  $V_{cmax}$ ,  $SLA$ , and  $CR_{s2l}$  have similar distributions between Par-CTR and Par-OBS. Compared with Par-CTR, Par-OBS has a narrower distribution of  $M_{bk}$  but broader distributions of  $WD$  and  $L_{leaf}$ .

Exp-CTR and Exp-OBS each include 1500 350-year ELM-FATES simulations. We averaged the last four years of these simulations for analysis, i.e., simulation outputs: Out-CTR and Out-OBS, respectively. To quantify the PFT coexistence, we computed the biomass ratio between early successional PFT and the total biomass, denoted as  $BR_{e2t}$ . For brevity, we denote the ELM-FATES experiments with  $BR_{e2t} \in [0.1, 0.9]$  as "coexistence",  $BR_{e2t} \in [0.0, 0.1)$  as "late",  $BR_{e2t} \in (0.9, 1.0]$  as "early". We calculated  $BR_{e2t}$  based on Out-CTR and Out-OBS, and then computed the fraction of coexistence experiments in each ensemble. As we will show in section 3.1, considering the observed trait relationships, Exp-OBS has a lower fraction of coexistence experiments. Therefore, only Exp-CTR was used for further ML-related analysis. We also

performed some analysis of Exp-CTR to explore whether the parameters of the coexistence experiments have correlations with each other (Section 3.2).

### **2.4.3 Procedure 3: ML surrogate models & sensitivity analysis**

Based on Exp-CTR, we trained XGBoost models to emulate the ELM-FATES model behavior and analyzed the parameter sensitivity (procedure "P3" in Figure 2). Sixteen variables were used as XGBoost model features, including 11 parameters in Par-CTR and 5 parameter differences between early and late successional PFTs. The corresponding ELM-FATES annual average outputs were used as XGBoost model targets. Specifically, six models were built, i.e., XGB\_ET, XGB\_SH, XGB\_BW, XGB\_GPP, XGB\_AGB, XGB\_BR for predicting ET, SH, BW, GPP, AGB, and  $BR_{e2t}$ , respectively. The ML models were trained, tested, and subsequently utilized to perform the parameter sensitivity analysis, as described in Section 2.5.

### **2.4.4 Procedure 4: ML surrogate models application & validation**

The trained XGBoost models were then used to help select ELM-FATES parameters (procedure "P4" in Figure 2). First, initial parameter sets were generated from procedure "P1" based on the entire eleven parameters' space (Table 1, identical to the parameters' space used for the generation of Par-CTR). Second, these parameter sets and parameter differences were sent to six XGBoost surrogate models to predict ET, SH, BW, GPP, AGB, and  $BR_{e2t}$ . Third, the predictions were further filtered by two criteria: (1) compared to observations, the relative biases of the predicted ET, SH, BW, GPP, and AGB should be less than 15%; (2) the XGBoost model predicted  $BR_{e2t}$  should be within [0.3, 0.7], which corresponds to the range where the XGB-BR model exhibited relatively better performance (Figure 5). We repeated these three steps until we obtained 1500 sets of XGBoost model predictions that matched the criteria. Finally, we obtained 1500 sets of XGBoost model predictions and their corresponding 1500 sets of parameters (Par-ML). We also

checked whether the selected Par-ML could match the empirical relationships derived from the empirical analysis in procedure "P2" (see Sections 3.2 and 3.5 for details). Then, the 1500 sets of parameters in Par-ML were sent to ELM-FATES to conduct 350-year runs (i.e., Exp-ML). The last four years of the simulations were averaged (i.e., Out-ML) for further analysis. We then filtered Out-ML based on a relative bias of 15% or less compared to observations and PFT coexistence to identify the optimal experiments and corresponding parameters.

## **2.5 ML model development and SHAP analysis**

The process of building each of the six ML surrogate models is described. Taking  $BR_{e2t}$  as an example, the 1500 pairs of sixteen features and the corresponding simulated  $BR_{e2t}$  were randomly split into two groups, 90% used for training and the remaining 10% used for testing. Given that the coexistence experiments only account for 20.6% in the simulations of Exp-CTR (Section 3.1), we used 90% of the data for training to ensure sufficient coexisting samples were included in the training process. Optimizing the hyperparameters of the XGBoost model is crucial for its performance. To achieve this, we employed the Bayesian optimization method during the training process (Snoek et al., 2012). In addition, to avoid overfitting during hyperparameter optimization, we utilized a five-fold cross-validation method (Feigl et al., 2021). The mean squared error was used as the objective function to achieve the optimal hyperparameters. The root mean squared error (RMSE) and R-squared ( $R^2$ ) are used to quantify the overall model performance for the training and testing data prediction.

Based on the trained XGBoost models, we subsequently employed a game theoretic approach called SHapley Additive exPlanations (SHAP; Lundberg and Lee, 2017; Lundberg et al., 2018, 2020) to gain insights into the parameter sensitivity of ELM-FATES. SHAP assumes that features

(predictive variables) interact and collaborate in a prediction game, with each feature receiving a payout for its contributions. This approach provides a unified measure of feature importance to explain both individual samples and the entire dataset, which is distinct from intrinsic feature importance methods such as the feature importance in XGBoost (Lundberg and Lee, 2017). This approach has been widely used in various fields, including interpreting a digital soil mapping model (Padarian et al., 2020) and identifying the critical drivers of wildfires (Wang et al., 2021). In this study, we performed SHAP analysis for each XGBoost model and used the SHAP values as a proxy to quantify the relative importance of ELM-FATES parameters.

### 3. Results

#### 3.1 Comparison between Exp-CTR and Exp-OBS

Constraining the input traits using the observed trait relationships yields slightly better ELM-FATES simulations of water, energy, and carbon variables (Figures 3a~3e). The distributions of the relative biases of ET, SH, BW, and GPP have similar ranges between the two sets of experiments (Figures 3a~3d). Compared with Exp-CTR, the 50<sup>th</sup> percentiles of relative biases of ET, SH, BW, and GPP for Exp-OBS (with constrained traits) are closer to zero, indicating Exp-OBS is slightly better than Exp-CTR. The distribution of simulated AGB for Exp-OBS is much narrower than Exp-CTR (Figure 3e), which could be due to the narrower distribution of  $M_{bk}$  (Figure S1).

Exp-CTR has a much higher fraction of PFT coexisting simulations than Exp-OBS (Figure 3f and Table S2). Overall, 70.6 % of experiments in Exp-CTR, and 94.5% of experiments in Exp-OBS have high simulated  $BR_{et}$  that is greater than 0.9. This indicates that both Par-CTR and especially Par-OBS favor the early successional PFT. As for the coexisting experiments with  $BR_{et} \in [0.1, 0.9]$ , Exp-CTR has about five times more coexisting experiments (20.6%) than Exp-OBS (4.1%). Further filtering the coexisting cases by observations (Table S1), only 21 experiments remain in Exp-CTR, and 6 experiments in Exp-OBS (Table S2). Even though Exp-OBS considered the observed trait relationships, it has fewer coexisting cases within the reasonable observation ranges than Exp-CTR. Therefore, Exp-OBS is not used in our remaining analysis.

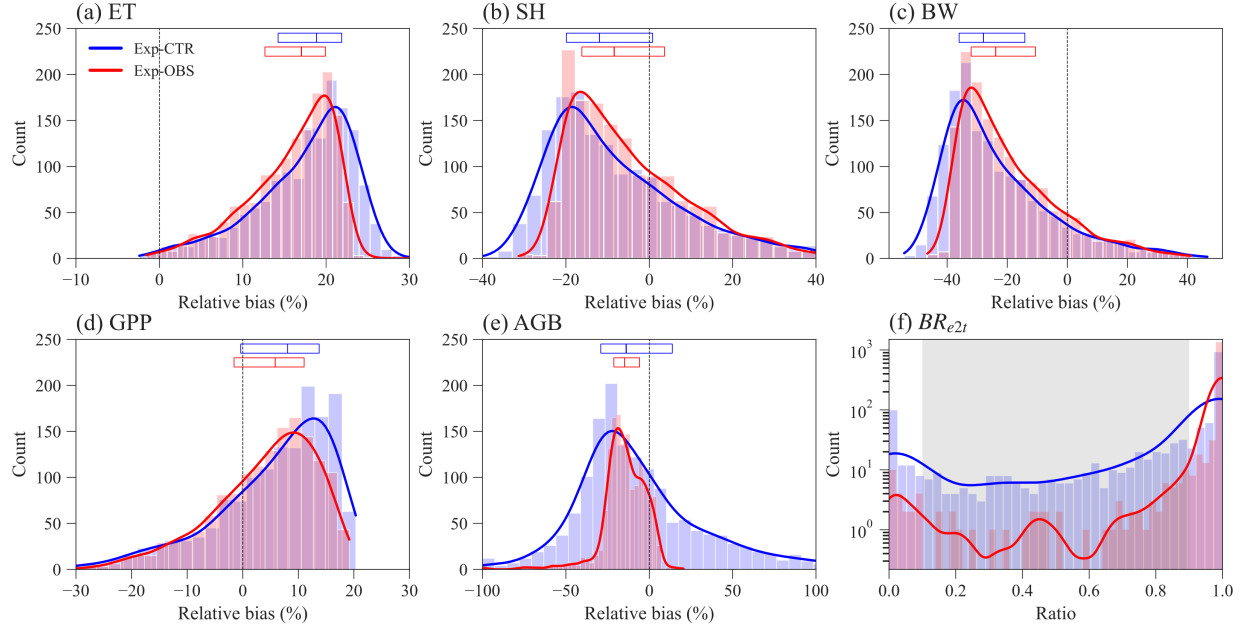


Figure 3. Distribution of ELM-FATES simulations for Exp-CTR and Exp-OBS. The y-axis in (f) is logarithmic.  $Relative\ bias = \frac{simulation - observation}{observation} \times 100\%$ . In (a)~(e), the top horizontal bars with three vertical lines denote the relative bias at the 25<sup>th</sup>, 50<sup>th</sup>, and 75<sup>th</sup> percentiles, respectively. The grey shaded area in (f) represents the coexistence biomass ratio between 0.1 and 0.9.

### 3.2 Parameter analysis of Exp-CTR

We also tested whether simple parameter correlations can be constructed to guide the simulation of PFTs coexistence. No simple parameter correlations can be built to distinguish the coexisting cases from the early and late cases in Exp-CTR (Figures 4, S2, and S3). Most parameter (or parameter difference) spaces show large overlaps between early, late, and coexisting cases (Figures S2 and S3). Notably, we empirically built three linear equations based on the boundaries in the parameter spaces for the coexisting cases (Figure 4). Coexisting cases are primarily located in spaces with  $SLA_{late} > 0.35 \times SLA_{early} + 0.003$  (Figures 4a and 4d),  $V_{cmax,diff} < -4800 \times SLA_{diff} + 100$  (Figures 4b and 4e), and  $WD_{diff} > 55 \times SLA_{diff} - 1.3$  (Figures 4c and 4f),



390 where  $V_{cmax,diff} = V_{cmax,early} - V_{cmax,late}$ , and  $SLA_{diff}$  and  $WD_{diff}$  are defined likewise.  
391 Within these constrained parameter spaces, the percentage of coexisting cases increases from the  
392 original 20.6% (i.e., 309 out of 1500) to 32.6% (i.e., 304 out of 932). Therefore, these empirical  
393 correlations could help guide ELM-FATES parameter selection for coexisting PFTs. On the other  
394 hand, a dominant proportion (i.e., 67.4% (1–32.6%)) of experiments are still either early or late  
395 cases within the constrained parameter spaces and cannot robustly predict PFT coexistence.  
396 Moreover, despite further considering the observational constraints (black scatters in Figure 4;  
397 Table S2), the 21 experiments (2.3%, 21 out of 932) are still sparsely distributed in the parameters'  
398 space of the coexisting cases, so no simple correlations can be developed based on these  
399 simulations. Therefore, simple empirically built relationships between plant traits provide limited  
400 benefit to guiding ELM-FATES parameter selection for modeling PFTs coexistence while  
401 matching the observations. This finding provides additional motivation for the ML-based  
402 approaches.

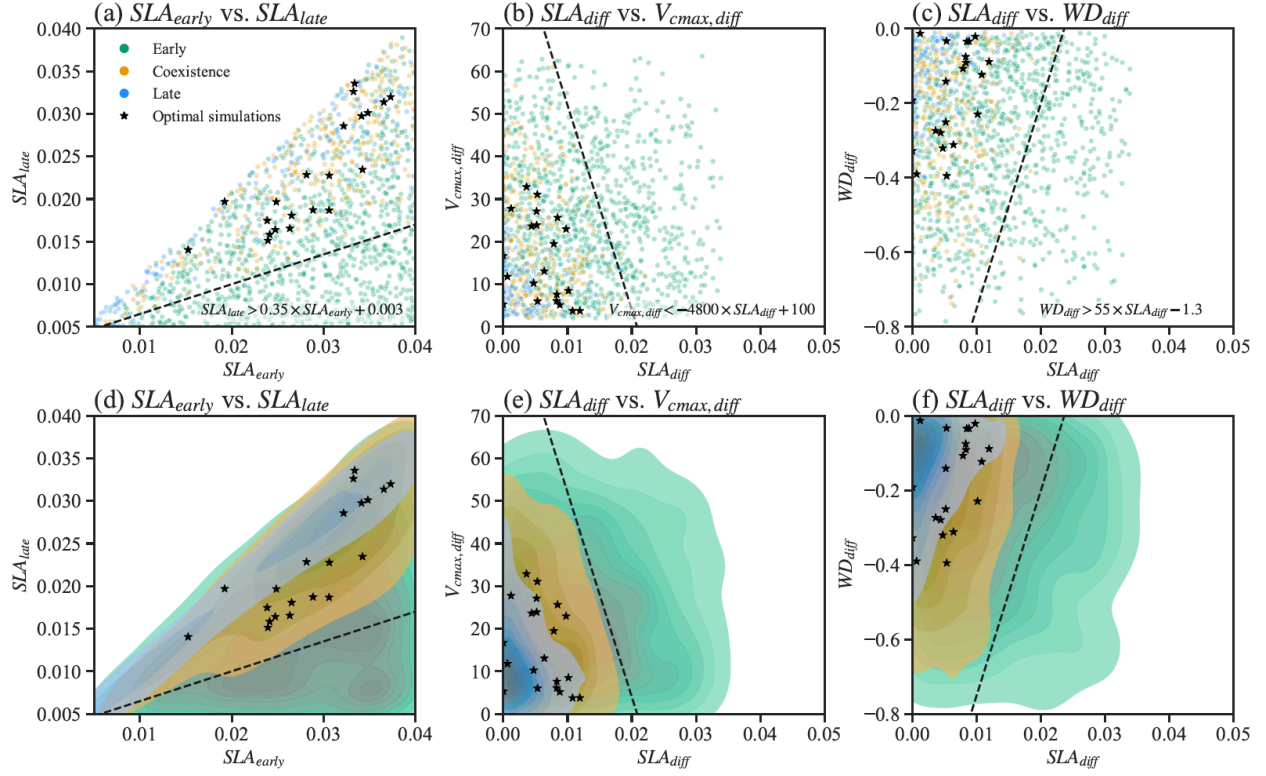


Figure 4. Relationships between selected parameters of Par-CTR. These parameters are presented in three groups, i.e., green color for the late cases with  $BR_{e2t} \in [0.0, 0.1)$ , orange color for the coexisting cases with  $BR_{e2t} \in [0.1, 0.9]$ , and blue color for the early cases with  $BR_{e2t} \in (0.9, 1.0]$ . Black star represents coexistence cases further filtered by observational constraints. (d)~(f) are the corresponding kernel density estimate plots of the scatter plots (a)~(c).  $V_{cmax,diff} = V_{cmax,early} - V_{cmax,late}$ .  $SLA_{diff}$  and  $WD_{diff}$  are defined likewise.

### 3.3 XGBoost model performance

Overall, the XGBoost surrogate models show good performance in predicting ELM-FATES simulations (Figure 5). Based on Exp-CTR (i.e., Par-CTR and Out-CTR), six XGBoost models were trained. In training, the RMSEs for the six models are zero or nearly zero, and  $R^2$ s are close to one. In the testing, four XGBoost models (i.e., XGB\_ET, XGB\_SH, XGB\_BW, XGB\_GPP)

still show good performance with small RMSE and large  $R^2$  ( $>0.95$ ). XGB\_AGB shows a little degradation with  $R^2$  of 0.88. The performance of XGB\_BR also shows degradation with  $R^2$  decreasing from 1.0 in training to 0.75 in testing. XGB\_BR cannot well predict the ELM-FATES simulated  $BR_{et}$  of 0 or 1 when only one PFT survives. This indicates that PFT competition processes in ELM-FATES, which determine  $BR_{et}$  and AGB, are highly nonlinear and difficult to emulate even using a state-of-the-art machine learning algorithm.

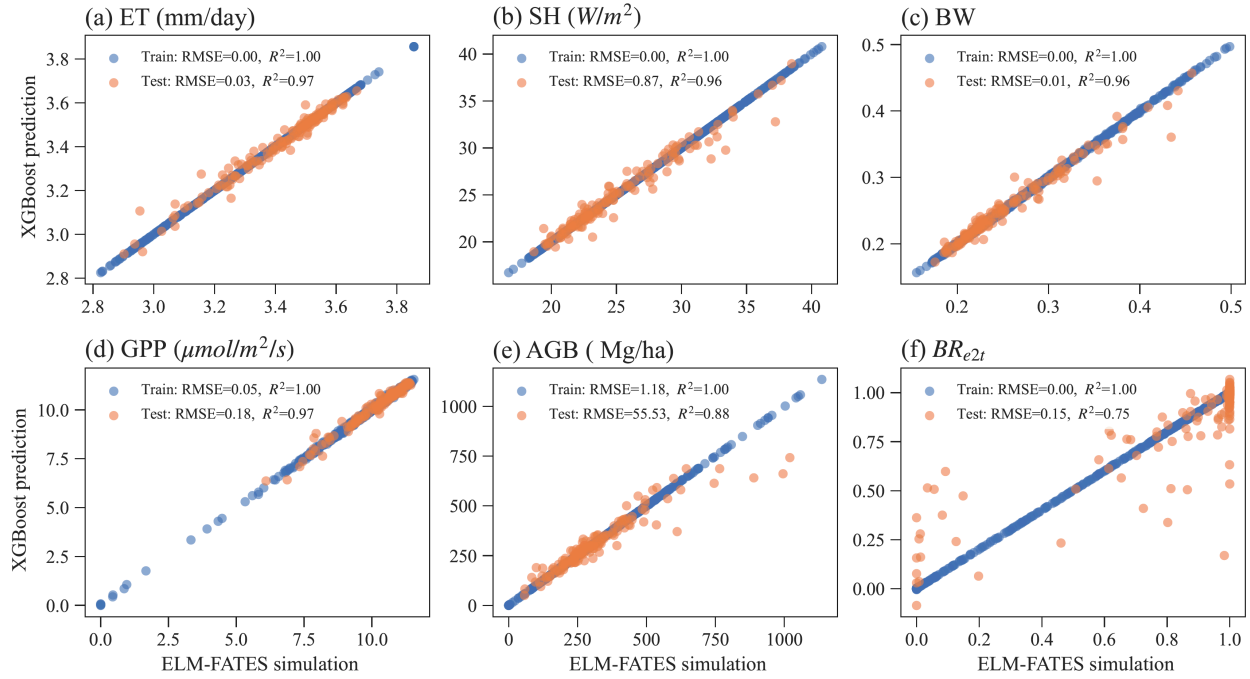


Figure 5. The performance of XGBoost surrogate models in the training and testing for predicting (a) ET, (b) SH, (c) BW, (d) GPP, (e) AGB, and (f)  $BR_{et}$ .

### 3.4 SHAP parameter importance analysis

Figure 6 shows the feature importance, including parameters and parameter differences, for different XGBoost models. Features (on the y-axis) with a higher mean absolute SHAP value (on the x-axis) denote a larger contribution to the XGBoost model prediction. The number of most

430 important features is different for predicting ET, SH, BW, and GPP compared with predicting  
 431 AGB and  $BR_{et}$ .  
 432 For the XGBoost models that predict ET, SH, BW, and GPP, the top three features have the largest  
 433 SHAP values compared to the rest (Figures 6a~5d). Notably, these top three features are the same  
 434 and correspond to the early successional PFT, i.e.,  $V_{cmax,early}$ ,  $SLA_{early}$ , and  $L_{leaf,early}$ . Most  
 435 ELM-FATES experiments in Exp-CTR used as the training samples for the XGBoost models are  
 436 early cases. Therefore, the parameters of early successional PFT have dominant contributions in  
 437 the XGBoost model predictions of overall grid-level fluxes. These three parameters are positively  
 438 correlated with ET and GPP and negatively correlated with SH and BW (red vs. blue bars in  
 439 Figures 6a~d; Figure S4 for more details), reflecting the fundamental carbon metabolism of the  
 440 typically dominant early successional plant.  
 441 For the XGBoost surrogate models of AGB and  $BR_{et}$ , more than eight features have large SHAP  
 442 values (Figures 6e and 6f). Both early and late successional PFT parameters contribute to  
 443 predicting the two variables. Compared with the predictions of ET, SH, BW, and GPP with only  
 444 three major features, predicting AGB and  $BR_{et}$  is relatively more complex. This is because AGB  
 445 and particularly  $BR_{et}$  are closely related to the PFT competition process in which both the early  
 446 and late PFT traits are crucial. Especially for  $BR_{et}$ , the most important features are the parameter  
 447 difference between the early and late successional PFTs. For example,  $SLA_{diff}$  is positively  
 448 correlated to  $BR_{et}$ . Therefore, to have coexisting PFTs with  $BR_{et} \in [0.1, 0.9]$ , the SLA of two  
 449 PFTs should neither be too large nor too small.

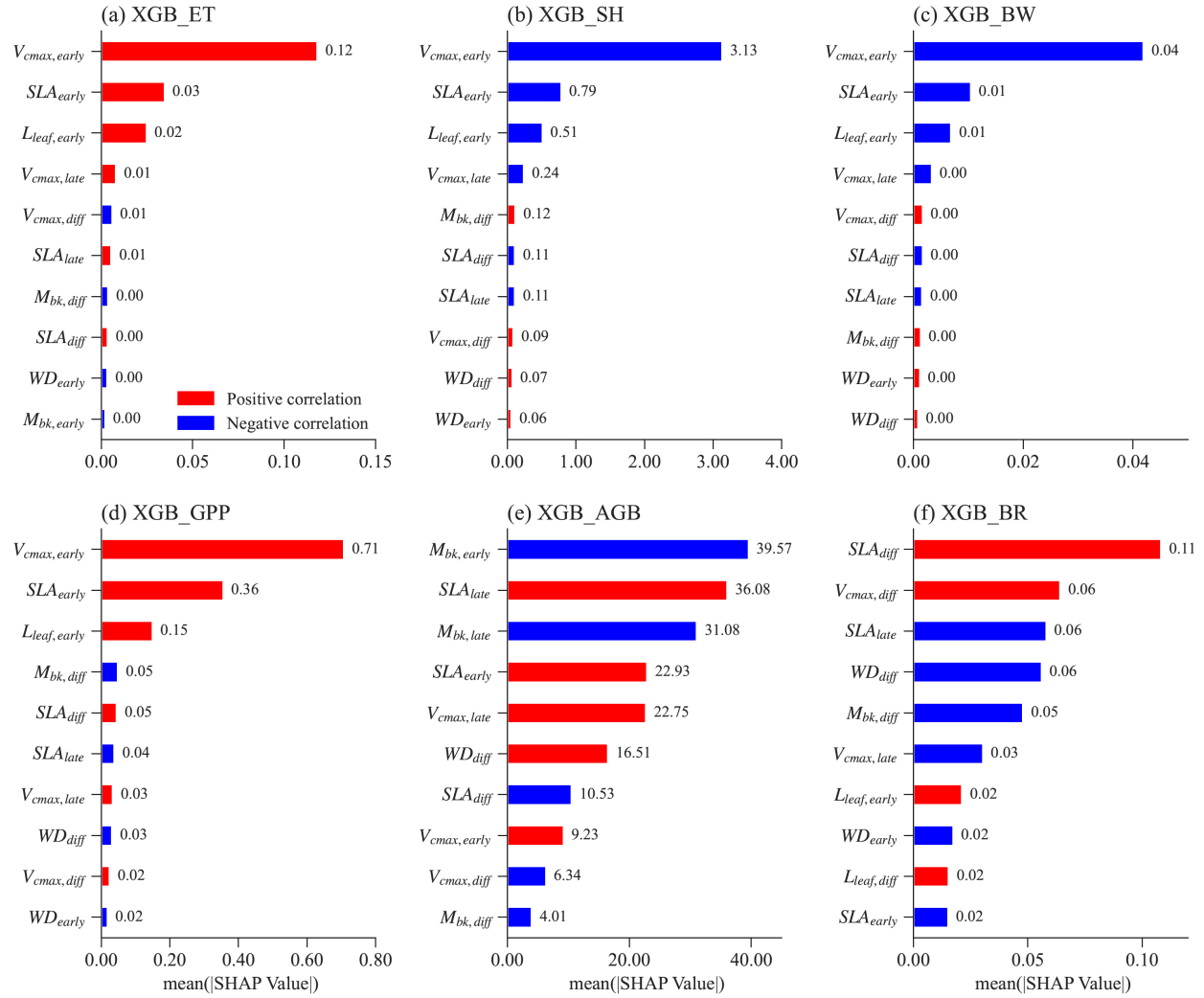


Figure 6. Mean absolute SHAP values for different XGBoost surrogate models for the top ten most important features. Absolute SHAP values are sorted in decreasing order from top to bottom. For each feature (y-axis) in each XGBoost model, the Spearman correlation coefficient is calculated between the feature values and the corresponding SHAP values (Figure S4). The red color means that a given feature is positively correlated with the predicting variable, whereas blue denotes a negative correlation.

### 3.5 XGBoost model parameter selection

Using the XGBoost surrogate models, the Par-ML was selected, including 1500 sets of parameters and the corresponding parameter differences between the early and late successional PFTs (Section 2.4, procedure "P4" in Figure 2). We examined whether Par-ML matches the empirical relationships shown in Figure 4 (Section 3.2), i.e.,  $SLA_{late} > 0.35 \times SLA_{early} + 0.003$ ,  $V_{cmax,diff} < -4800 \times SLA_{diff} + 100$ , and  $WD_{diff} > 55 \times SLA_{diff} - 1.3$ . In total, 99.1% (1486 out of 1500) of parameter sets are consistent with the empirical relationships, indicating the XGBoost models implicitly learned these simple relationships.

The parameter distributions of Par-ML show different patterns from the early/late parameters of Par-CTR (green vs. blue regions in Figure 7), but there are large overlaps between the coexistence parameters of Par-CTR and Par-ML (orange vs. green regions, e.g., the third column in Figure 7). This indicates that the XGBoost surrogate models learned to select parameters around the parameters' space of the coexisting cases. Par-ML also tends to have a smaller parameter difference between the early and late successional PFTs in terms of  $SLA_{diff}$  and  $V_{cmax,diff}$ . However, Par-ML also shows different patterns from the coexisting parameters of Par-CTR, probably because the XGBoost selected parameters were also constrained by multiple observations and implicitly considered parameter tradeoffs. For example, the  $V_{cmax,early}$  and  $V_{cmax,late}$  of Par-ML are located in narrower ranges than the coexisting parameters of Par-CTR (first two columns in Figure 7).

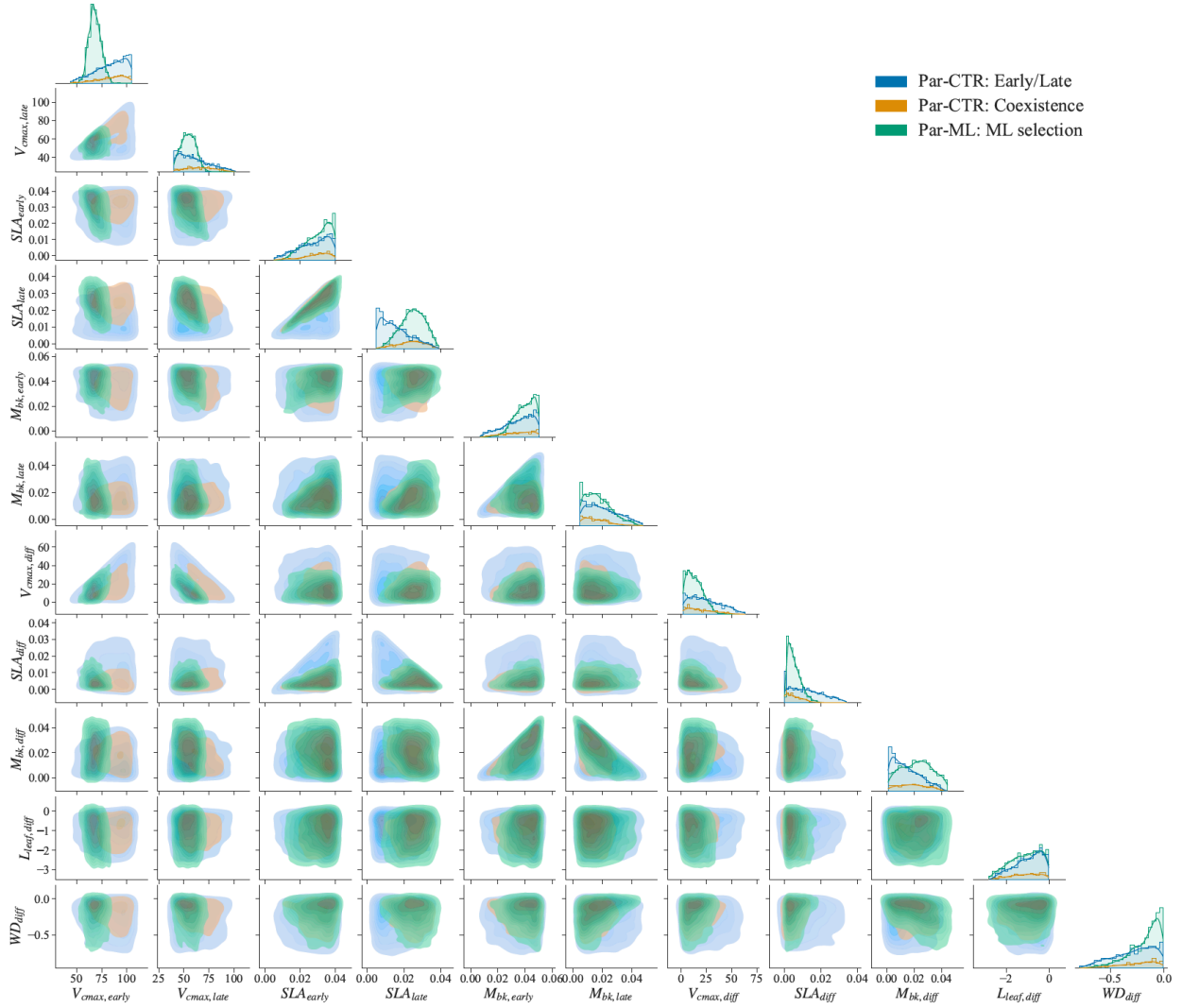


Figure 7. Comparison of parameter or parameter difference in Par-CTR vs. Par-ML for eleven features. The diagonal plots represent each parameter's distribution, and the rest of the subplots are kernel density estimate plots. There are three groups, i.e., blue for the early/late cases of Par-CTR, orange for the coexisting cases of Par-CTR, and green for Par-ML selected by XGBoost models.

### 3.6 Validation of ML selected parameters

ELM-FATES simulations of Exp-ML based on the ensemble parameters of Par-ML selected by the XGBoost surrogate models can better capture the observations and have more coexisting cases than Exp-CTR (Figure 8). The median values of simulated variables for Exp-ML are closer to observations with relative biases closer to zero than Exp-CTR (Figure 8a, blue vs. green boxes). The Exp-ML simulated variables also have more concentrated distributions than Exp-CTR. Compared to the skewed distribution of  $BR_{e2t}$  in Exp-CTR with a large proportion of early cases, Exp-ML has a more normally distributed  $BR_{e2t}$  (Figure 8b). Specifically, Exp-ML has about 3.6 times more coexisting cases than Exp-CTR, i.e., 73.1% (1097 out of 1500) in Exp-ML vs. 20.6% (309 out of 1500) in Exp-CTR (Table S3). After being further constrained by observation (Table S3), one-third of the experiments (i.e., 495 out of 1500) in Exp-ML remain, and this ratio is 23.6 times more than 1.4% (21 out of 1500) in Exp-CTR.

The XGBoost surrogate model predicted variables also match well with those simulated using ELM-FATES in Exp-ML (Figure 8, orange vs. green boxes), indicating the overall reasonable accuracy for the XGBoost model predictions. Compared to the ELM-FATES results using Par-ML, the XGBoost models show better performance for ET, SH, BW, and GPP, but relatively degraded performance for AGB and  $BR_{e2t}$  (Figure S5). It is consistent with the performance of the XGBoost models' training and testing results (in Section 3.3).



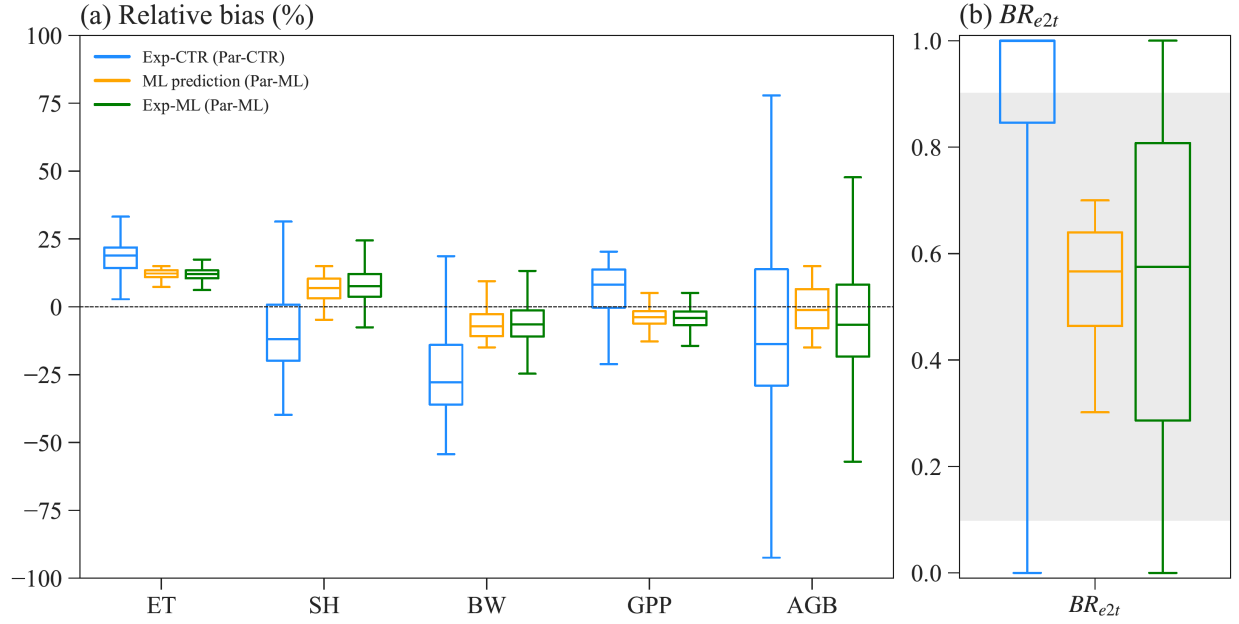


Figure 8. Comparison between the ELM-FATES simulations for Exp-CTR and Exp-ML. (a) Relative bias for simulated ET, SH, BW, GPP, and AGB. (b) Simulated  $BR_{e2t}$ . ML prediction represents the selected XGBoost model predictions after filtering with observation and biomass ratio (i.e., the XGB\_prds, procedure "P4" in Figure 2).

### 3.7 Parameter tradeoff for coexistence experiments

Parameters of the early and late successional PFTs show tradeoffs for the coexisting experiments. Large relative differences in  $SLA$ ,  $V_{cmax}$ , and  $WD$  (more negative) favor the early successional PFT, while large relative differences in  $M_{bk}$  and  $L_{leaf}$  favor the late successional PFT. Therefore, in Exp-CTR, compared to the early and late cases, the coexisting cases have intermediate relative differences in  $SLA$ ,  $V_{cmax}$ ,  $WD$ ,  $M_{bk}$ , and  $L_{leaf}$  (dashed boxes in Figure 9). The coexisting cases in Exp-ML have similar patterns with intermediate relative differences in  $SLA$ ,  $V_{cmax}$  and  $L_{leaf}$  compared to the early and late cases (solid boxes in Figure 9). However,  $M_{bk}$  and especially  $WD$  show the largest relative difference for the coexisting cases compared to the early and late cases

in Exp-ML. These two parameters still show a tradeoff in determining coexisting PFTs, because larger  $WD$  favors the early PFT while larger  $M_{bk}$  favors the late PFT.

In Exp-ML, the parameter spaces of the coexisting cases show large overlaps with the early/late cases (Figure S6). There are no simple correlations between these parameters to distinguish the coexisting cases from the early and late cases (also see Section 3.2). Although  $WD_{diff}$  of the coexisting cases still overlap with the early/late cases, when  $WD_{diff}$  is less than roughly  $-0.4$  ( $\text{g/cm}^3$ ), only coexisting cases exist (Figure S6). Nevertheless, this rule (i.e.,  $WD_{diff} < -0.4$ ) alone cannot ensure PFT coexistence (see Figure 7).

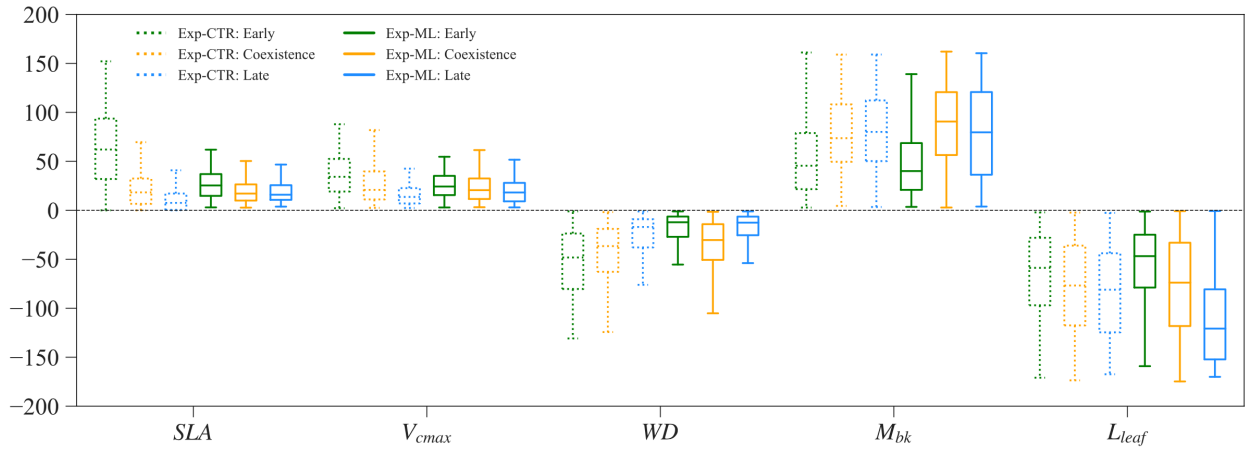


Figure 9. Parameter relative difference (%) between early successional PFT and late successional PFT for Exp-CTR (box with dash line) and Exp-ML (box with solid line). Parameter relative difference is calculated as, taking SLA as an example,  $\frac{SLA_{early} - SLA_{late}}{(SLA_{early} + SLA_{late})/2} \times 100$  (%).

### 3.8 Seasonal variation comparison

Figure 10 shows the seasonal variations of ET, SH, BW, and GPP for observations and simulations of the finally selected 495 experiments in Exp-ML with good model performance (Table S3). Overall, the simulated ET shows a similar seasonal variation to ET observation (Figure 10a), with relatively small ET in the wet season (November–May), high ET in the dry season (June–October), and ET peaks in August. However, compared to the observations, ELM-FATES overestimates ET, especially during the wet season. The simulated SH also shows a similar seasonal variation with the SH observation except in March. ELM-FATES overestimated SH from January to May but underestimated SH from September to December (Figure 10b). Due to the discrepancy between simulated ET and SH, the model underestimates BW from September to December (Figure 10c). The simulated GPP has minor seasonal variability compared to the observed GPP. ELM-FATES overestimates GPP from June–August in the dry season, but underestimates GPP over October–December. The lower GPP over June–August indicates that plants may be relatively water-stressed or energy limited during these months. However, the large ET observation over the same period implies that this site is unlikely water limited or strongly energy limited. The ELM-FATES simulations also display little water stress year-round (Figure S7). Therefore, there are likely elements of the seasonal cycle (e.g., phenological responses of photosynthetic capacity) that are not yet captured here. Additionally, tower estimates of GPP may also have large uncertainties.

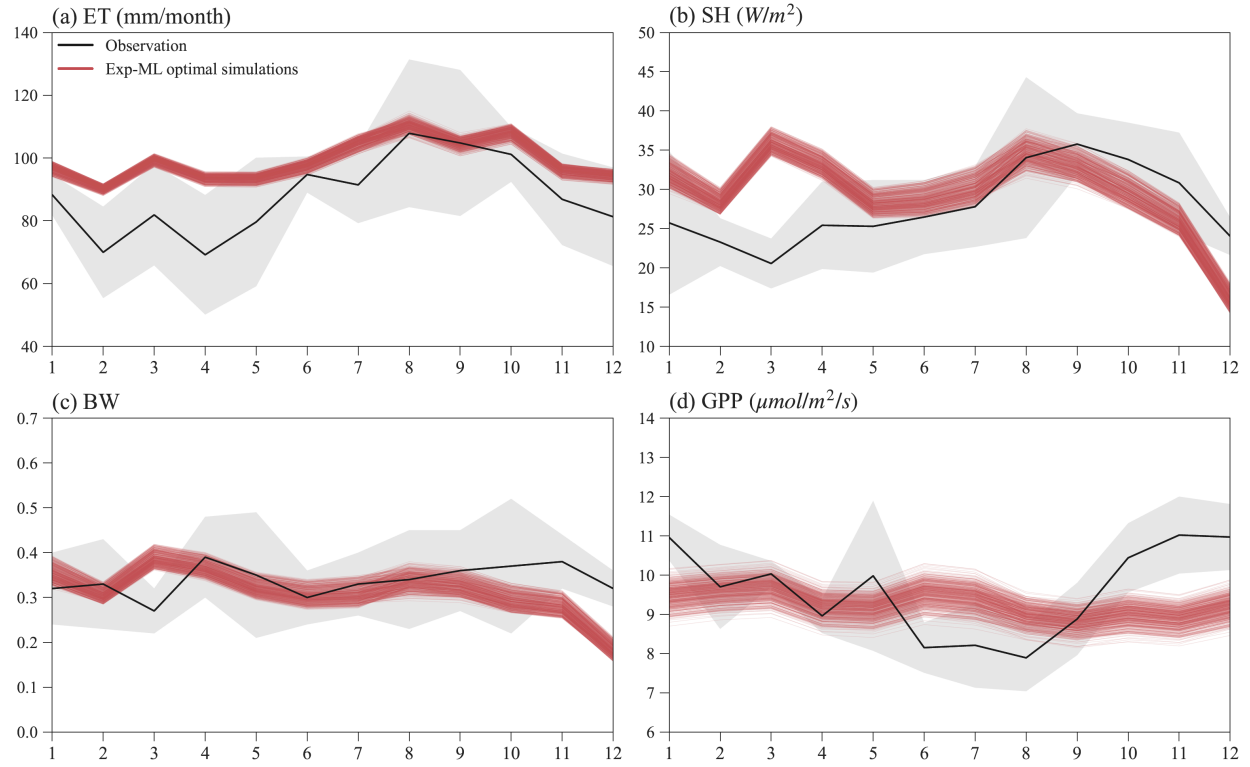


Figure 10. Mean monthly observations and selected optimal ELM-FATES simulations in Exp-ML for (a) ET, (b) SH, (c) BW, and (d) GPP. Each red line represents one experiment simulation (four-year simulation average). The black curves are monthly climatologic averages from 2000 to 2008, and the grey shaded area represents the interannual variabilities (i.e., *mean*  $\pm$  *standard deviation*).

## 4. Discussion

### 4.1 Limited guidance of observed trait relationships for PFT coexistence modeling in FATES

We found degraded PFT coexistence in ELM-FATES simulation when observed trait relationships are considered. More specifically, constrained by observed trait relationships, Exp-OBS has fewer coexisting cases than Exp-CTR which does not consider the observed trait relationships. The observed trait relationships were derived from site measurements in the species-rich tropical ecosystem where plant coexistence commonly happens (Kraft et al., 2008), which is expected to enhance the PFT coexistence simulations. This inconsistency could be due to several possible reasons. First, ELM-FATES is a typical "trait filtering" model (Fisher et al., 2018), and the realistic simulation of PFT dynamics largely depends on the fidelity with which trait tradeoff surfaces are prescribed in the model (Scheiter et al., 2012). Implicit representation of trait tradeoff in the current ELM-FATES model may not be well balanced, which may differ from the observed trait relationships that lead to coexistence in the real world (at least for the ecosystem at our study site). In particular, there may be correlated tradeoffs that are measured (e.g., with below ground processes, Chitra-Tarak et al. 2021) but not represented in the model. A second reason could be the mismatch between different spatial scales. The observed trait relationships are derived from field measurements across tropical forests over a large region with diverse species and climate, e.g., the relationship in equation (1) is for plant species in Panama. In contrast, ELM-FATES simulations were conducted at the K34 site scale with specific species composition. Therefore, the large-scale trait relationships may not reflect the small-scale trait relationships. Wright et al. (2005) showed that trait relationships fitted for individual sites varied considerably. Third, the observed trait relationships are based on simplified equations, which may not be able to comprehensively reflect PFT coexistence. For example, although equation (2) derived from Longo et al. (2020) can

reflect the negative relationship between SLA and  $L_{leaf}$ , the  $R^2$  of this equation is about 0.49, which may not be accurate enough to represent trait relationships. Additionally, these equations (1)~(3) do not consider the uncertainty of traits covariance. In Koven et al. (2020), the uncertainties between trait covariance were considered when sampling parameters for FATES experiments. Furthermore, machine learning models can also be employed to extract the relationships between plant traits, which can then be incorporated into ELM-FATES and evaluated in future studies.

#### **4.2 Advantages of ML surrogate models on improving PFT coexistence modeling**

ELM-FATES simulations driven by parameters selected using the XGBoost models essentially improved PFT coexistence and better captured observations. Compared to the initial Exp-CTR, which was used to train the XGBoost models, the proportion of coexisting PFTs in Exp-ML reaches 73.1%, 3.6 times more than 20.6% in Exp-CTR. Further filtering the coexistence experiments by observations, Exp-ML still has 33.0% of experiments left with good model performance, 23.6 times that of 1.4% of experiments in Exp-CTR with good performance. Our ML-based approach also outperforms the empirical correlations built in Section 3.2, which only yields 32.5% of coexistence experiments and this reduces to 2.3% of experiments if further constrained by observation. The large proportion of optimal experiments selected by our ML approach also outperforms previous studies using direct filtering approaches. Buotte et al. (2021) conducted two stages of experiments to select optimal parameters for CLM-FATES modeling with two conifer species; only 0.3% (1 out of 360) of the cases met the given criteria in the first stage experiments, which increased to 5.5% in the second stage experiments. Huang et al. (2020) conducted CLM-FATES modeling with two tropical PFTs at the Tapajós National Forest sites; only one parameter set out of seventy (about 1.4%) was selected with reasonable fractions of two

PFTs and minor errors compared to observations. In addition, the parameter selection procedures of these two studies require some degree of subjective decision making and expert knowledge. On the other hand, our ML-based approach takes a more objective procedure, and little expert knowledge is required except for the initial determination of the parameter reference ranges. Importantly, we believe this approach can be repeatable as, e.g., model developments lead to changes between the parameter values and model predictions of forest structure and function, and can be used to define constrained ensemble values that will allow assessment of confidence in model predictions. Even though simulating the coexistence of different plants may not be a big concern for individual-based VDMs, e.g., LPJmL-FIT (Sakschewski et al., 2015, 2016) and TROLL (Maréchaux and Chave, 2017), our approach also could be applied to the selection of key parameters that regulate vegetation dynamics in these models.

Our study also reproduced the observations satisfactorily. Holm et al. (2020) conducted the ELM-FATES simulation with only one PFT considered at the same K34 site. Our study yields better or similar performance in the magnitude of AGB, and the magnitude and seasonal variation of GPP, ET, SH, and BW (Table 2 and Figure 3 in Holm et al. 2020 vs. Figures 8 and 10 in this study). It should also be noted that the overestimation of simulated energy fluxes (latent heat and SH) from January to May could be associated with the energy-related processes (e.g., energy partition, surface albedo) in ELM-FATES. Other potential reasons could be related to the uncertainties in atmospheric forcing and the common issue of incomplete energy budget closure at eddy covariance towers (Wilson et al., 2002; Foken, 2008; Rocha et al., 2009).

Compared to the predictions of GPP, ET, SH, and BW simulated by ELM-FATES, the XGBoost surrogate models show slightly degraded performance in predicting the simulated  $BR_{et}$  and AGB (Figures 5 and S5). Three parameters ( $V_{cmax,early}$ ,  $SLA_{early}$ , and  $L_{leaf,early}$ ) mainly control the predictions of ET, SH, BW, and GPP, while eight features are crucial for predicting AGB and  $BR_{et}$ . Even though the XGBoost algorithm has an excellent ability to capture complex nonlinear relationships, it does not predict well the PFT competition related variables of AGB and  $BR_{et}$  because the physical model cannot robustly predict coexisting PFTs due to the higher dimensionality of predicting PFT composition as compared to other ecosystem variables. Another important point worth mentioning is the small sample size of coexistence cases in Exp-CTR, with only 309 cases having  $BR_{et}$  in the range of [0.1, 0.9], while the majority of cases are dominated by either early or late successional PFT. This limited sample size may not provide enough data to train the XGBoost surrogate model sufficiently for predicting  $BR_{et}$  within the range of [0.1, 0.9]. Therefore, further studies are still needed to improve the emulation of PFT competition related variables. Other approaches that have been applied in VDMs but not specifically for PFT coexistence modeling, for example, the generalized likelihood uncertainty estimation (GLUE) approach (Zhang et al., 2022) and the Bayesian model emulation approach (Fer et al., 2018), could provide alternative ways. Furthermore, we suggest exploring other machine learning algorithms, such as Gaussian process and neural network algorithms, which may be better suited for capturing non-linear correlations and learning from sparse data.

Overall, our study presents a reproducible approach that utilizes machine learning to identify parameter values that improve model fidelity against observations and promote coexistence between plant functional types in vegetation demography models across diverse ecosystems. This



approach has the potential to enhance the modeling of PFT coexistence in other ecosystems, such as the mixed conifer forests in Sierra Nevada, California (Buotte et al., 2021), Amazon forests subject to selective logging (Huang et al., 2020) and tropical forests with heterogeneous soils and subject to droughts in Panama (Cheng et al., 2021).

### 4.3 Trait tradeoffs between coexisting PFTs

Trait-related parameters show tradeoffs between early and late successional PFTs for the ELM–FATES simulated coexisting experiments. The relative differences between the two PFTs in  $SLA$ ,  $V_{cmax}$ , and  $WD$  complementarily coordinate with the relative difference in  $M_{bk}$  and  $L_{leaf}$ , hence avoiding competitive exclusion (Figure 9). These ELM-FATES reflected tradeoffs are consistent with the niche-based species coexistence mechanisms of environmental filtering and niche partitioning (MICHALKO and PEKÁR, 2015; Adler et al., 2013). On the one hand, in the coexisting cases, the relative differences between the two PFTs' parameters should not be considerable. For example, a large difference in  $SLA$  more likely favors the early cases (green dash box in Figure 9). This is related to environmental filtering in which coexisting species require some degree of convergence in strategy to survive and persist under given environmental conditions (Cadotte and Tucker, 2017; Thakur and Wright, 2017). On the other hand, some degree of differences should exist between the two PFTs' parameters in the coexisting cases. This is related to niche partitioning to ensure either differences in resource requirements or differences in tolerance to surrounding conditions (Kraft et al., 2015; Fowler et al., 2013). Phenomenological evidence has shown that functional trait variation promotes coexistence or increases species richness (Uriarte et al., 2010; Angert et al., 2009; Adler et al., 2006; Mason et al., 2012; Ben-Hur et al., 2012).

665

666 In our ELM-FATES simulations, the primary axis of competition for resources is light. The  
667 tradeoffs between the two PFTs' parameters differentiate their vertical competition in light  
668 absorption, which has been shown to strongly control tropical forest community composition  
669 (Farrior et al., 2016; Poorter et al., 2003). Even though the early PFT has a shallower rooting depth  
670 than the late PFT, there is no critical dry condition during our simulation period (i.e., corresponding  
671 to values of the water stress factor (BTRAN) close to 1.0 in Figure S7). Therefore, competition for  
672 water resource access negligibly contributes to PFT coexistence in this study. Previous tropical  
673 studies also revealed these coexistence mechanisms. At a tropical forest site in eastern Ecuador,  
674 Kraft et al. (2008) found that cooccurring trees are often less ecologically similar, and both  
675 environmental filtering (different topographic habitats of ridgetops vs. valley) and niche  
676 differentiation simultaneously contribute to species coexistence. Swenson & Enquist (2009) also  
677 found that at small spatial scales in a tropical forest, most traits of coexisting species were under-  
678 dispersed, consistent with environmental filtering, while the seed mass and maximum height were  
679 over-dispersed, reflecting niche partitioning.

680

#### 681 **4.4 Limitations and further model development**

682 Some limitations exist in our experiments. Niche partitioning is a critical aspect of promoting  
683 species coexistence, which is closely related to spatial heterogeneity, temporal heterogeneity,  
684 disturbances (e.g., nature enemy, fire), and resource partitioning (Adler et al., 2013). In our current  
685 ELM-FATES simulations, some processes that have been or are being developed in the model are  
686 not considered. These processes include nutrient limitation (Holm et al., 2020), fire disturbance  
687 (Fisher et al., 2015), subsurface lateral flow (Fang et al., 2022), and plant hydraulics (Chitra-Tarak

et al., 2021; Li et al., 2021). Ignoring these processes could limit the potential of niche partitioning among PFT in our ELM-FATES simulations. Topography has been recognized as an essential spatial heterogeneity factor for tropical forests, but it is not considered in ELM-FATES (Kraft et al., 2008; Costa et al., 2022). For example, Fang et al. (2022) coupled a three-dimensional hydrology model (ParFlow) with ELM-FATES and found that lateral flow plays a prominent role in governing aboveground biomass, and Cheng et al. (2021) also found a critical role for subsurface hydrology on coexistence. As these processes are added to the model, the reproducibility aspects of the XGBoost method to identify PFT combinations that match a broad range of criteria will be particularly important.

Lacking other features or processes could also affect PFT coexistence in the current FATES. For example, plant trait plasticity, that plants can adjust their morphological and/or physiological traits to better adapt to the environment (Nicotra et al., 2010; Bloomfield et al., 2018; McDowell et al., 2022), is also not well considered in FATES. Leaf traits such as  $V_{cmax}$  and SLA do vary vertically through the canopy in FATES, via a prescribed relationship described by Lloyd et al., 2010. Liu and Ng (2019) found that the SLA of a desert shrub is significantly correlated with seasonal water availability. Additionally, FATES only considers the inter-PFT variance of functional traits (e.g., different  $V_{cmax}$  for early and late PFT). However, studies revealed that trait variations commonly exist within and between species (Wright et al., 2005; Engemann et al., 2016; Meng et al., 2015; Dong et al., 2020; Siefert et al., 2015), which play a vital role in maintaining plant diversity (Violle et al., 2012; Lu et al., 2017). Reproductive features that enhance competitive exclusion tendencies have been illustrated to affect coexistence (Maréchaux and Chave, 2017; Fisher et al., 2018). Hanbury-Brown et al. (2022) discussed the importance of the representation of forest regeneration,

including improving parameters and algorithms for reproductive allocation, dispersal, seed survival and germination, environmental filtering in the seedling layer, and tree regeneration strategies adapted to wind, fire, and anthropogenic disturbance regimes. Besides, both growth-survival and stature-recruitment tradeoffs are critical to accurately predict successional patterns in tropical forest structure and competition (see details in Rüger et al., 2020), which should also be better considered in future model development. Furthermore, measured plant traits are increasingly available, e.g., the TRY datasets (Kattge et al., 2020) can be used to improve the model process and parameterizations. Future studies on properly and adequately using these datasets to guide VDM parameterizations are advocated.

#### **4.5 Enhancing VDM prediction with machine learning**

We provide a brief overview of how machine learning can be applied to improve the modeling of plant dynamics, specifically in the context of vegetation demographic models. Firstly, ML can be used to derive trait parameter values. For instance, in this study, ML could be applied to replace the simple equations to derive the relationships between measured traits (Section 4.1). By integrating multiple datasets, including in situ measurements, atmospheric forcing, and remote sensing, ML could derive the spatial patterns and temporal variations of trait parameters for use in large-scale VDM modeling. Secondly, ML can be utilized to optimize parameters by developing surrogate models that emulate the relationships between the parameters and the VDM simulations, and using the surrogate models to identify optimal parameter values. This application has demonstrated success in this study and previous studies (e.g., Tsai et al., 2021; Dagon et al., 2020; Watson-Parris et al., 2021). Another benefit of using ML in VDMs is the ability to develop benchmark datasets. For example, studies have successfully employed ML to derive AGB datasets

734 for various ecosystems (Morais et al., 2021; Zhang et al., 2020; Li et al., 2020; Bispo et al., 2020;  
735 Pham et al., 2020). These datasets can serve as benchmarks to evaluate the accuracy of VDM  
736 simulations. Lastly, ML can be used to replace semiempirical sub-models with little theoretical  
737 bases in DGVMs (Reichstein et al., 2019). For example, accurately modeling wildfire using  
738 process-based wildfire models integrated in DGVMs remains challenging. However, ML-based  
739 wildfire models have shown advantages in accuracy and computational efficiency (Rodrigues and  
740 Riva, 2014; Jain et al., 2020; Sayad et al., 2019), and have the potential to be employed in Earth  
741 system models to improve wildfire simulations (e.g., Zhu et al., 2022).

## 5. Conclusions

In this study, we explored two possible solutions to improve PFT coexistence modeling in a cohort-based model (ELM-FATES): (1) using plant trait relationships established from field measurements and (2) using machine learning surrogate models to optimize trait parameter values. Three ensembles of ELM-FATES experiments were conducted over a tropical forest site at Manaus, Brazil. We found that considering the observed trait relationships (Exp-OBS) slightly improves the simulations of water (ET), energy (SH and BW), and carbon (GPP, AGB) when compared against observations, but degrades the simulation of PFT coexistence. Based on Exp-CTR, the ML surrogate models were built to optimize the ELM-FATES parameters by integrating the observations (i.e., ET, SH, BW, GPP, and AGB) and PFT coexistence criteria. Exp-ML, with parameters selected by the ML surrogate models, vastly improves the simulation of PFT coexistence, and also better reproduces the annual means and seasonal variations of ET, SH, BW, GPP, and the field inventory of AGB. This study demonstrates the benefits of using machine learning models to improve the modeling of PFT coexistence in ELM-FATES, with important implications for modeling the response and feedback of ecosystem dynamics to climate change. Our results also suggest that the incorporation of additional mechanisms into ELM-FATES is essential for robust modeling of coexisting PFTs.

*Code and Data Availability.* The ELM-FATES source code, surface and domain data, forcing data, and ML codes used in this study are archived on Zenodo (<https://doi.org/10.5281/zenodo.7730685>). The observational reference datasets of GPP, ET, SH, BW, and AGB are obtained from Holm et al. (2020). The forcing data are available from Oak Ridge National Laboratory Distributed Active Archive Center (ORNL DAAC), LBA-ECO CD-32 Flux Tower Network Data Compilation, Brazilian Amazon: 1999-2006, V2, [https://daac.ornl.gov/LBA/guides/CD32\\_Fluxes\\_Brazil.html](https://daac.ornl.gov/LBA/guides/CD32_Fluxes_Brazil.html).

*Author contributions.* LL and YF designed and conducted the experiments and analysis, and drafted the manuscript. ZZ and MS contributed to the machine learning, experiment design, and improvement of the manuscript. LRL contributed to the interpretation and discussion of results, and improvement of the manuscript. ML, CDK, JAH, RF, NGM, and JC contributed to the dataset, interpretation, discussion, and modification of the manuscript.

*Acknowledgments.* This research was conducted at Pacific Northwest National Laboratory, operated for the U.S. Department of Energy by Battelle Memorial Institute under contract DE-AC05-76RL01830. This study was supported by the Department of Energy's (DOE) Office of Biological and Environmental Research as part of the Terrestrial Ecosystem Science program through the Next-Generation Ecosystem Experiments (NGEE)-Tropics project. RF acknowledges funding by the European Union's Horizon 2020 (H2020) research and innovation program under Grant Agreement No. 101003536 (ESM2025 – Earth System Models for the Future) and 821003 (4C, Climate-Carbon Interactions in the Coming Century)

782 *Financial support.* This research was supported by the U.S. Department of Energy, Office of  
783 Science (grant no. 71073).  
784 *Competing interests.* The authors declare that they have no conflict of interest.



## Reference

- Adler, P. B., HilleRisLambers, J., Kyriakidis, P. C., Guan, Q., and Levine, J. M.: Climate variability has a stabilizing effect on the coexistence of prairie grasses., *P Natl Acad Sci Usa*, 103, 12793–8, <https://doi.org/10.1073/pnas.0600599103>, 2006.
- Adler, P. B., Fajardo, A., Kleinhesselink, A. R., and Kraft, N. J. B.: Trait-based tests of coexistence mechanisms, *Ecol Lett*, 16, 1294–1306, <https://doi.org/10.1111/ele.12157>, 2013.
- Angert, A. L., Huxman, T. E., Chesson, P., and Venable, D. L.: Functional tradeoffs determine species coexistence via the storage effect, *Proc National Acad Sci*, 106, 11641–11645, <https://doi.org/10.1073/pnas.0904512106>, 2009.
- Antoniadis, A., Lambert-Lacroix, S., and Poggi, J.-M.: Random forests for global sensitivity analysis: A selective review, *Reliab Eng Syst Safe*, 206, 107312, <https://doi.org/10.1016/j.res.2020.107312>, 2020.
- Bauman, D., Fortunel, C., Delhay, G., Malhi, Y., Cernusak, L. A., Bentley, L. P., Rifai, S. W., Aguirre-Gutiérrez, J., Menor, I. O., Phillips, O. L., McNellis, B. E., Bradford, M., Laurance, S. G. W., Hutchinson, M. F., Dempsey, R., Santos-Andrade, P. E., Ninantay-Rivera, H. R., Paucar, J. R. C., and McMahon, S. M.: Tropical tree mortality has increased with rising atmospheric water stress, *Nature*, 1–6, <https://doi.org/10.1038/s41586-022-04737-7>, 2022.
- Belda, D. M., Anthoni, P., Wärlind, D., Olin, S., Schurgers, G., Tang, J., Smith, B., and Arneth, A.: LPJ-GUESS/LSMv1.0: a next-generation land surface model with high ecological realism, *Geosci Model Dev*, 15, 6709–6745, <https://doi.org/10.5194/gmd-15-6709-2022>, 2022.
- Ben-Hur, E., Fragman-Sapir, O., Hadas, R., Singer, A., and Kadmon, R.: Functional trade-offs increase species diversity in experimental plant communities, *Ecol Lett*, 15, 1276–1282, <https://doi.org/10.1111/j.1461-0248.2012.01850.x>, 2012.
- Berzaghi, F., Wright, I. J., Kramer, K., Oddou-Muratorio, S., Bohn, F. J., Reyer, C. P. O., Sabaté, S., Sanders, T. G. M., and Hartig, F.: Towards a New Generation of Trait-Flexible Vegetation Models, *Trends Ecol Evol*, 35, 191–205, <https://doi.org/10.1016/j.tree.2019.11.006>, 2019.
- Bispo, P. da C., Rodríguez-Veiga, P., Zimbres, B., Miranda, S. do C. de, Cezare, C. H. G., Fleming, S., Baldacchino, F., Louis, V., Rains, D., Garcia, M., Espírito-Santo, F. D. B., Roitman, I., Pacheco-Pascagaza, A. M., Gou, Y., Roberts, J., Barrett, K., Ferreira, L. G., Shimbo, J. Z., Alencar, A., Bustamante, M., Woodhouse, I. H., Sano, E. E., Ometto, J. P., Tansey, K., and Balzter, H.: Woody Aboveground Biomass Mapping of the Brazilian Savanna with a Multi-Sensor and Machine Learning Approach, *Remote Sens*, 12, 2685, <https://doi.org/10.3390/rs12172685>, 2020.

820 Bloomfield, K. J., Cernusak, L. A., Eamus, D., Ellsworth, D. S., Prentice, I. C., Wright, I. J.,  
821 Boer, M. M., Bradford, M. G., Cale, P., Cleverly, J., Egerton, J. J. G., Evans, B. J., Hayes, L. S.,  
822 Hutchinson, M. F., Liddell, M. J., Macfarlane, C., Meyer, W. S., Prober, S. M., Togashi, H. F.,  
823 Wardlaw, T., Zhu, L., and Atkin, O. K.: A continental-scale assessment of variability in leaf  
824 traits: Within species, across sites and between seasons, *Funct Ecol*, 32, 1492–1506,  
825 <https://doi.org/10.1111/1365-2435.13097>, 2018.

826 Bonan, G. B.: Forests and Climate Change: Forcings, Feedbacks, and the Climate Benefits of  
827 Forests, *Science*, 320, 1444–1449, <https://doi.org/10.1126/science.1155121>, 2008.

828 Breiman, L.: Random Forests, *Mach Learn*, 45, 5–32, <https://doi.org/10.1023/a:1010933404324>,  
829 2001.

830 Brister, E., Newhouse, A. E., and Texas, C. for E. P., The University of North: Not the Same Old  
831 Chestnut: Rewilding Forests with Biotechnology, *Environ Ethics*, 42, 149–167,  
832 <https://doi.org/10.5840/enviroethics2020111614>, 2020.

833 Buotte, P. C., Koven, C. D., Xu, C., Shuman, J. K., Goulden, M. L., Levis, S., Katz, J., Ding, J.,  
834 Ma, W., Robbins, Z., and Kueppers, L. M.: Capturing functional strategies and compositional  
835 dynamics in vegetation demographic models, *Biogeosciences*, 18, 4473–4490,  
836 <https://doi.org/10.5194/bg-18-4473-2021>, 2021.

837 Cadotte, M. W. and Tucker, C. M.: Should Environmental Filtering be Abandoned?, *Trends Ecol*  
838 *Evol*, 32, 429–437, <https://doi.org/10.1016/j.tree.2017.03.004>, 2017.

839 Cao, M. and Woodward, F. I.: Dynamic responses of terrestrial ecosystem carbon cycling to  
840 global climate change, *Nature*, 393, 249–252, <https://doi.org/10.1038/30460>, 1998.

841 Chen, T. and Guestrin, C.: XGBoost: A Scalable Tree Boosting System, *Proc 22nd Acm Sigkdd*  
842 *Int Conf Knowl Discov Data Min*, 785–794, <https://doi.org/10.1145/2939672.2939785>, 2016.

843 Cheng, Y., Leung, L. R., Huang, M., Koven, C., Detto, M., Knox, R., Bisht, G., Bretfeld, M., and  
844 Fisher, R. A.: Modeling the joint effects of vegetation characteristics and soil properties on  
845 ecosystem dynamics in a Panama tropical forest, *J Adv Model Earth Sy*,  
846 <https://doi.org/10.1029/2021ms002603>, 2021.

847 Chitra-Tarak, R., Xu, C., Aguilar, S., Anderson-Teixeira, K. J., Chambers, J., Detto, M.,  
848 Faybishenko, B., Fisher, R. A., Knox, R. G., Koven, C. D., Kueppers, L. M., Kunert, N., Kupers,  
849 S. J., McDowell, N. G., Newman, B. D., Paton, S. R., Pérez, R., Ruiz, L., Sack, L., Warren, J.  
850 M., Wolfe, B. T., Wright, C., Wright, S. J., Zailaa, J., and McMahon, S. M.: Hydraulically-  
851 vulnerable trees survive on deep-water access during droughts in a tropical forest, *New Phytol*,  
852 231, 1798–1813, <https://doi.org/10.1111/nph.17464>, 2021.

853 Christoffersen, B. O., Gloor, M., Fauset, S., Fyllas, N. M., Galbraith, D. R., Baker, T. R., Kruijt,  
854 B., Rowland, L., Fisher, R. A., Binks, O. J., Sevanto, S., Xu, C., Jansen, S., Choat, B.,  
855 Mencuccini, M., McDowell, N. G., and Meir, P.: Linking hydraulic traits to tropical forest

function in a size-structured and trait-driven model (TFS v.1-Hydro), *Geoscientific Model Development*, 9, 4227–4255, <https://doi.org/10.5194/gmd-9-4227-2016>, 2016.

Costa, F. R. C., Schietti, J., Stark, S. C., and Smith, M. N.: The other side of tropical forest drought: do shallow water table regions of Amazonia act as large-scale hydrological refugia from drought?, *New Phytol*, <https://doi.org/10.1111/nph.17914>, 2022.

Dagon, K., Sanderson, B. M., Fisher, R. A., and Lawrence, D. M.: A machine learning approach to emulation and biophysical parameter estimation with the Community Land Model, version 5, *Adv Statistical Clim Meteorology Oceanogr*, 6, 223–244, <https://doi.org/10.5194/ascmo-6-223-2020>, 2020.

Díaz, S., Kattge, J., Cornelissen, J. H. C., Wright, I. J., Lavorel, S., Dray, S., Reu, B., Kleyer, M., Wirth, C., Prentice, I. C., Garnier, E., Bönsch, G., Westoby, M., Poorter, H., Reich, P. B., Moles, A. T., Dickie, J., Gillison, A. N., Zanne, A. E., Chave, J., Wright, S. J., Sheremet’ev, S. N., Jactel, H., Baraloto, C., Cerabolini, B., Pierce, S., Shipley, B., Kirkup, D., Casanoves, F., Joswig, J. S., Günther, A., Falczuk, V., Rüger, N., Mahecha, M. D., and Gorné, L. D.: The global spectrum of plant form and function, *Nature*, 529, 167–171, <https://doi.org/10.1038/nature16489>, 2016.

Domingues, T. F., Berry, J. A., Martinelli, L. A., Ometto, J. P. H. B., and Ehleringer, J. R.: Parameterization of Canopy Structure and Leaf-Level Gas Exchange for an Eastern Amazonian Tropical Rain Forest (Tapajós National Forest, Pará, Brazil), *Earth Interact*, 9, 1–23, <https://doi.org/10.1175/ei149.1>, 2005.

Dong, N., Prentice, I. C., Wright, I. J., Evans, B. J., Togashi, H. F., Caddy-Retalic, S., McInerney, F. A., Sparrow, B., Leitch, E., and Lowe, A. J.: Components of leaf-trait variation along environmental gradients, *New Phytol*, 228, 82–94, <https://doi.org/10.1111/nph.16558>, 2020.

Duan, Q., Sorooshian, S., and Gupta, V.: Effective and efficient global optimization for conceptual rainfall-runoff models, *Water Resour Res*, 28, 1015–1031, <https://doi.org/10.1029/91wr02985>, 1992.

Engemann, K., Sandel, B., Boyle, B., Enquist, B. J., Jørgensen, P. M., Kattge, J., McGill, B. J., Morueta-Holme, N., Peet, R. K., Spencer, N. J., Violle, C., Wiser, S. K., and Svenning, J.-C.: A plant growth form dataset for the New World., *Ecology*, 97, 3243–3243, <https://doi.org/10.1002/ecy.1569>, 2016.

Fang, Y., Leung, L. R., Duan, Z., Wigmosta, M. S., Maxwell, R. M., Chambers, J. Q., and Tomasella, J.: Influence of landscape heterogeneity on water available to tropical forests in an Amazonian catchment and implications for modeling drought response, *Journal of Geophysical Research: Atmospheres*, 122, 8410–8426, <https://doi.org/10.1002/2017jd027066>, 2017.

Fang, Y., Leung, R., Koven, C., Bisht, G., Detto, M., Cheng, Y., McDowell, N., Muller-Landau, H., Wright, S. J., and Chambers, J.: Modeling the topographic influence on aboveground

893 biomass using a coupled model of hillslope hydrology and ecosystem dynamics, *Geoscientific*  
894 *Model Dev Discuss*, 2022, 1–41, <https://doi.org/10.5194/gmd-2022-148>, 2022.

895 Farrior, C. E., Bohlman, S. A., Hubbell, S., and Pacala, S. W.: Dominance of the suppressed:  
896 Power-law size structure in tropical forests, *Science*, 351, 155–157,  
897 <https://doi.org/10.1126/science.aad0592>, 2016.

898 Feeley, K. J., Davies, S. J., Ashton, P. S., Bunyavejchewin, S., Supardi, M. N. N., Kassim, A. R.,  
899 Tan, S., and Chave, J.: The role of gap phase processes in the biomass dynamics of tropical  
900 forests, *Proc Royal Soc B Biological Sci*, 274, 2857–2864,  
901 <https://doi.org/10.1098/rspb.2007.0954>, 2007.

902 Feigl, M., Lebedzinski, K., Herrnegger, M., and Schulz, K.: Machine-learning methods for  
903 stream water temperature prediction, *Hydrol Earth Syst Sc*, 25, 2951–2977,  
904 <https://doi.org/10.5194/hess-25-2951-2021>, 2021.

905 Fer, I., Kelly, R., Moorcroft, P. R., Richardson, A. D., Cowdery, E. M., and Dietze, M. C.:  
906 Linking big models to big data: efficient ecosystem model calibration through Bayesian model  
907 emulation, *Biogeosciences*, 15, 5801–5830, <https://doi.org/10.5194/bg-15-5801-2018>, 2018.

908 Fisher, R., McDowell, N., Purves, D., Moorcroft, P., Sitch, S., Cox, P., Huntingford, C., Meir, P.,  
909 and Woodward, F. I.: Assessing uncertainties in a second-generation dynamic vegetation model  
910 caused by ecological scale limitations, *New Phytol*, 187, 666–681,  
911 <https://doi.org/10.1111/j.1469-8137.2010.03340.x>, 2010.

912 Fisher, R. A., Muszala, S., Versteinstein, M., Lawrence, P., Xu, C., McDowell, N. G., Knox, R.  
913 G., Koven, C., Holm, J., Rogers, B. M., Spessa, A., Lawrence, D., and Bonan, G.: Taking off the  
914 training wheels: the properties of a dynamic vegetation model without climate envelopes,  
915 *CLM4.5(ED)*, *Geosci Model Dev*, 8, 3593–3619, <https://doi.org/10.5194/gmd-8-3593-2015>,  
916 2015.

917 Fisher, R. A., Koven, C. D., Anderegg, W. R. L., Christoffersen, B. O., Dietze, M. C., Farrior, C.  
918 E., Holm, J. A., Hurtt, G. C., Knox, R. G., Lawrence, P. J., Lichstein, J. W., Longo, M.,  
919 Matheny, A. M., Medvigy, D., Muller-Landau, H. C., Powell, T. L., Serbin, S. P., Sato, H.,  
920 Shuman, J. K., Smith, B., Trugman, A. T., Viskari, T., Verbeeck, H., Weng, E., Xu, C., Xu, X.,  
921 Zhang, T., and Moorcroft, P. R.: Vegetation demographics in Earth System Models: A review of  
922 progress and priorities, *Global Change Biol*, 24, 35–54, <https://doi.org/10.1111/gcb.13910>, 2018.

923 Foken, T.: THE ENERGY BALANCE CLOSURE PROBLEM: AN OVERVIEW, *Ecol Appl*,  
924 18, 1351–1367, <https://doi.org/10.1890/06-0922.1>, 2008.

925 Foley, J. A., Prentice, I. C., Ramankutty, N., Levis, S., Pollard, D., Sitch, S., and Haxeltine, A.:  
926 An integrated biosphere model of land surface processes, terrestrial carbon balance, and  
927 vegetation dynamics, *Global Biogeochem Cy*, 10, 603–628, <https://doi.org/10.1029/96gb02692>,  
928 1996.

929 Fowler, D., Lessard, J.-P., and Sanders, N. J.: Niche filtering rather than partitioning shapes the  
930 structure of temperate forest ant communities., *J Animal Ecol*, 83, 943–52,  
931 <https://doi.org/10.1111/1365-2656.12188>, 2013.

932 Friedman, J. H.: Greedy function approximation: A gradient boosting machine., *Ann Statistics*,  
933 29, <https://doi.org/10.1214/aos/1013203451>, 2001.

934 Fyllas, N. M., Gloor, E., Mercado, L. M., Sitch, S., Quesada, C. A., Domingues, T. F., Galbraith,  
935 D. R., Torre-Lezama, A., Vilanova, E., Ramírez-Angulo, H., Higuchi, N., Neill, D. A., Silveira,  
936 M., Ferreira, L., C, G. A. A., MALHI, Y., Phillips, O. L., and Lloyd, J.: Analysing Amazonian  
937 forest productivity using a new individual and trait-based model (TFS v.1), *Geoscientific Model*  
938 *Development*, 7, 1251–1269, <https://doi.org/10.5194/gmd-7-1251-2014>, 2014.

939 Gatti, L. V., Basso, L. S., Miller, J. B., Gloor, M., Domingues, L. G., Cassol, H. L. G., Tejada,  
940 G., Aragão, L. E. O. C., Nobre, C., Peters, W., Marani, L., Arai, E., Sanches, A. H., Corrêa, S.  
941 M., Anderson, L., Randow, C. V., Correia, C. S. C., Crispim, S. P., and Neves, R. A. L.:  
942 Amazonia as a carbon source linked to deforestation and climate change, *Nature*, 595, 388–393,  
943 <https://doi.org/10.1038/s41586-021-03629-6>, 2021.

944 Golaz, J., Caldwell, P. M., Roedel, L. P. V., Petersen, M. R., Tang, Q., Wolfe, J. D., Abeshu, G.,  
945 Anantharaj, V., Asay-Davis, X. S., Bader, D. C., Baldwin, S. A., Bisht, G., Bogenschütz, P. A.,  
946 Branstetter, M., Brunke, M. A., Brus, S. R., Burrows, S. M., Cameron-Smith, P. J., Donahue, A.  
947 S., Deakin, M., Easter, R. C., Evans, K. J., Feng, Y., Flanner, M., Foucar, J. G., Fyke, J. G.,  
948 Griffin, B. M., Hannay, C., Harrop, B. E., Hoffman, M. J., Hunke, E. C., Jacob, R. L., Jacobsen,  
949 D. W., Jeffery, N., Jones, P. W., Keen, N. D., Klein, S. A., Larson, V. E., Leung, L. R., Li, H.,  
950 Lin, W., Lipscomb, W. H., Ma, P., Mahajan, S., Maltrud, M. E., Mametjanov, A., McClean, J.  
951 L., McCoy, R. B., Neale, R. B., Price, S. F., Qian, Y., Rasch, P. J., Eyre, J. E. J. R., Riley, W. J.,  
952 Ringler, T. D., Roberts, A. F., Roesler, E. L., Salinger, A. G., Shaheen, Z., Shi, X., Singh, B.,  
953 Tang, J., Taylor, M. A., Thornton, P. E., Turner, A. K., Veneziani, M., Wan, H., Wang, H.,  
954 Wang, S., Williams, D. N., Wolfram, P. J., Worley, P. H., Xie, S., Yang, Y., Yoon, J., Zelinka,  
955 M. D., Zender, C. S., Zeng, X., Zhang, C., Zhang, K., Zhang, Y., Zheng, X., Zhou, T., and Zhu,  
956 Q.: The DOE E3SM Coupled Model Version 1: Overview and Evaluation at Standard  
957 Resolution, *J Adv Model Earth Sy*, 11, 2089–2129, <https://doi.org/10.1029/2018ms001603>,  
958 2019.

959 Hanbury-Brown, A. R., Ward, R. E., and Kueppers, L. M.: Forest regeneration within Earth  
960 system models: current process representations and ways forward, *New Phytol*, 235, 20–40,  
961 <https://doi.org/10.1111/nph.18131>, 2022.

962 Haverd, V., Smith, B., Cook, G. D., Briggs, P. R., Nieradzik, L., Roxburgh, S. H., Liedloff, A.,  
963 Meyer, C. P., and Canadell, J. G.: A stand-alone tree demography and landscape structure  
964 module for Earth system models, *Geophys Res Lett*, 40, 5234–5239,  
965 <https://doi.org/10.1002/grl.50972>, 2013.

966 He, X., Liu, S., Xu, T., Yu, K., Gentine, P., Zhang, Z., Xu, Z., Jiao, D., and Wu, D.: Improving  
 967 predictions of evapotranspiration by integrating multi-source observations and land surface  
 968 model, *Agr Water Manage*, 272, 107827, <https://doi.org/10.1016/j.agwat.2022.107827>, 2022.

969 Holm, J. A., Knox, R. G., Zhu, Q., Fisher, R. A., Koven, C. D., Lima, A. J. N., Riley, W. J.,  
 970 Longo, M., Negrón-Juárez, R. I., Araujo, A. C., Kueppers, L. M., Moorcroft, P. R., Higuchi, N.,  
 971 and Chambers, J. Q.: The Central Amazon Biomass Sink Under Current and Future Atmospheric  
 972 CO<sub>2</sub>: Predictions From Big-Leaf and Demographic Vegetation Models, *J Geophys Res*  
 973 *Biogeosciences*, 125, <https://doi.org/10.1029/2019jg005500>, 2020.

974 Huang, M., Xu, Y., Longo, M., Keller, M., Knox, R. G., Koven, C. D., and Fisher, R. A.:  
 975 Assessing impacts of selective logging on water, energy, and carbon budgets and ecosystem  
 976 dynamics in Amazon forests using the Functionally Assembled Terrestrial Ecosystem Simulator,  
 977 *Biogeosciences*, 17, 4999–5023, <https://doi.org/10.5194/bg-17-4999-2020>, 2020.

978 Hubau, W., Lewis, S. L., Phillips, O. L., Affum-Baffoe, K., Beeckman, H., Cuní-Sánchez, A.,  
 979 Daniels, A. K., Ewango, C. E. N., Fauset, S., Mukinzi, J. M., SHEIL, D., Sonké, B., Sullivan, M.  
 980 J. P., Sunderland, T. C. H., Taedoumg, H., Thomas, S. C., White, L. J. T., Abernethy, K. A.,  
 981 Adu-Bredu, S., Amani, C. A., Baker, T. R., Banin, L. F., Baya, F., Begne, S. K., Bennett, A. C.,  
 982 Benedet, F., Bitariho, R., Bocko, Y. E., Boeckx, P., Boundja, P., Brien, R. J. W., Brncic, T.,  
 983 Chezeaux, E., Chuyong, G. B., Clark, C. J., Collins, M., Comiskey, J. A., Coomes, D. A.,  
 984 Dargie, G. C., Haulleville, T. de, Kamdem, M. N. D., Doucet, J.-L., Esquivel-Muelbert, A.,  
 985 Feldpausch, T. R., Fofanah, A., Foli, E. G., Gilpin, M., Gloor, E., Gonmadje, C., Gourlet-Fleury,  
 986 S., Hall, J. S., Hamilton, A. C., Harris, D. J., Hart, T. B., Hockemba, M. B. N., Hladik, A., Ifo, S.  
 987 A., Jeffery, K. J., Jucker, T., Yakusu, E. K., Kearsley, E., Kenfack, D., Koch, A., Leal, M. E.,  
 988 Levesley, A., Lindsell, J. A., Lisingo, J., González, G. L., Lovett, J. C., Makana, J.-R., Malhi, Y.,  
 989 Marshall, A. R., Martin, J., Martin, E. H., Mbayu, F. M., Medjibe, V. P., Mihindou, V.,  
 990 Mitchard, E. T. A., Moore, S., Munishi, P. K. T., Bengone, N. N., Ojo, L., Ondo, F. E., Peh, K.  
 991 S. H., Pickavance, G. C., Poulsen, A. D., Poulsen, J. R., Qie, L., Reitsma, J., Rovero, F., Swaine,  
 992 M. D., Talbot, J., Taplin, J., Taylor, D. M., Thomas, D. W., Toirambe, B., Mukendi, J. T.,  
 993 Tuagben, D., Umunay, P. M., et al.: Asynchronous carbon sink saturation in African and  
 994 Amazonian tropical forests, *Nature*, 579, 80–87, <https://doi.org/10.1038/s41586-020-2035-0>,  
 995 2020.

996 Hurtt, G. C., Moorcroft, P. R., And, S. W. P., and Levin, S. A.: Terrestrial models and global  
 997 change: challenges for the future, *Global Change Biol*, 4, 581–590,  
 998 <https://doi.org/10.1046/j.1365-2486.1998.101-1-00203.x>, 1998.

999 Jain, P., Coogan, S. C. P., Subramanian, S. G., Crowley, M., Taylor, S., and Flannigan, M. D.: A  
 1000 review of machine learning applications in wildfire science and management, *Arxiv*,  
 1001 <https://doi.org/10.48550/arxiv.2003.00646>, 2020.

1002 Jonard, M., André, F., Coligny, F. de, Wergifosse, L. de, Beudez, N., Davi, H., Ligot, G.,  
 1003 Ponette, Q., and Vincke, C.: HETEROFOR 1.0: a spatially explicit model for exploring the  
 1004 response of structurally complex forests to uncertain future conditions – Part 1: Carbon fluxes



1005 and tree dimensional growth, *Geosci Model Dev*, 13, 905–935, [https://doi.org/10.5194/gmd-13-](https://doi.org/10.5194/gmd-13-905-2020)  
1006 [905-2020](https://doi.org/10.5194/gmd-13-905-2020), 2020.

1007 Jung, M., Koirala, S., Weber, U., Ichii, K., Gans, F., Camps-Valls, G., Papale, D., Schwalm, C.,  
1008 Tramontana, G., and Reichstein, M.: The FLUXCOM ensemble of global land-atmosphere  
1009 energy fluxes., *Sci Data*, 6, 74, <https://doi.org/10.1038/s41597-019-0076-8>, 2019.

1010 Kattge, J., Bönisch, G., Díaz, S., Lavorel, S., Prentice, I. C., Leadley, P., Tautenhahn, S., Werner,  
1011 G. D. A., Aakala, T., Abedi, M., Acosta, A. T. R., Adamidis, G. C., Adamson, K., Aiba, M.,  
1012 Albert, C. H., Alcántara, J. M., C. C. A., Aleixo, I., Ali, H., Amiaud, B., Ammer, C., Amoroso,  
1013 M. M., Anand, M., Anderson, C., Anten, N., Antos, J., Apgaua, D. M. G., Ashman, T. L.,  
1014 Asmara, D. H., Asner, G. P., Aspinwall, M., Atkin, O., Aubin, I., Spohr, L. B., Bahalkeh, K.,  
1015 Bahn, M., Baker, T., Baker, W. J., Bakker, J. P., Baldocchi, D., Baltzer, J., Banerjee, A.,  
1016 Baranger, A., Barlow, J., Barneche, D. R., Baruch, Z., Bastianelli, D., Battles, J., Bauerle, W.,  
1017 Bauters, M., Bazzato, E., Beckmann, M., Beeckman, H., Beierkuhnlein, C., Bekker, R., Belfry,  
1018 G., Belluau, M., Beloiu, M., Benavides, R., Benomar, L., Lattke, M. L. B., Berenguer, E.,  
1019 Bergamin, R., Bergmann, J., Carlucci, M. B., Berner, L., Römermann, M. B., Bigler, C.,  
1020 Bjorkman, A. D., Blackman, C., Blanco, C., Blonder, B., Blumenthal, D., González, K. T. B.,  
1021 Boeckx, P., Bohlman, S., Gaese, K. B., Marsh, L. B., Bond, W., Bond-Lamberty, B., Boom, A.,  
1022 Boonman, C. C. F., Bordin, K., Boughton, E. H., Boukili, V., Bowman, D. M. J. S., Bravo, S.,  
1023 Brendel, M. R., Broadley, M. R., Brown, K. A., Bruelheide, H., Brumnich, F., Bruun, H. H.,  
1024 Bruy, D., Buchanan, S. W., Bucher, S. F., Buchmann, N., Buitenwerf, R., Bunker, D. E., et al.:  
1025 TRY plant trait database – enhanced coverage and open access, *Global Change Biology*, 26,  
1026 119–188, <https://doi.org/10.1111/gcb.14904>, 2020.

1027 Koven, C. D., Knox, R. G., Fisher, R. A., Chambers, J. Q., Christoffersen, B. O., Davies, S. J.,  
1028 Detto, M., Dietze, M. C., Faybishenko, B., Holm, J., Huang, M., Kovenock, M., Kueppers, L.  
1029 M., Lemieux, G., Massoud, E., McDowell, N. G., Muller-Landau, H. C., Needham, J. F., Norby,  
1030 R. J., Powell, T., Rogers, A., Serbin, S. P., Shuman, J. K., Swann, A. L. S., Varadharajan, C.,  
1031 Walker, A. P., Wright, S. J., and Xu, C.: Benchmarking and parameter sensitivity of  
1032 physiological and vegetation dynamics using the Functionally Assembled Terrestrial Ecosystem  
1033 Simulator (FATES) at Barro Colorado Island, Panama, *Biogeosciences*, 17, 3017–3044,  
1034 <https://doi.org/10.5194/bg-17-3017-2020>, 2020.

1035 Kraft, N. J. B., Valencia, R., and Ackerly, D. D.: Functional Traits and Niche-Based Tree  
1036 Community Assembly in an Amazonian Forest, *Science*, 322, 580–582,  
1037 <https://doi.org/10.1126/science.1160662>, 2008.

1038 Kraft, N. J. B., Adler, P. B., Godoy, O., James, E. C., Fuller, S., and Levine, J. M.: Community  
1039 assembly, coexistence and the environmental filtering metaphor, *Funct Ecol*, 29, 592–599,  
1040 <https://doi.org/10.1111/1365-2435.12345>, 2015.

1041 Lambert, M. S. A., Tang, H., Aas, K. S., Stordal, F., Fisher, R. A., Fang, Y., Ding, J., and  
1042 Parmentier, F.-J. W.: Inclusion of a cold hardening scheme to represent frost tolerance is  
1043 essential to model realistic plant hydraulics in the Arctic–boreal zone in CLM5.0-FATES-Hydro,  
1044 *Geosci Model Dev*, 15, 8809–8829, <https://doi.org/10.5194/gmd-15-8809-2022>, 2022.

1045 Lawrence, D. M., Fisher, R. A., Koven, C. D., Oleson, K. W., Swenson, S. C., Bonan, G.,  
1046 Collier, N., Ghimire, B., Kampenhout, L., Kennedy, D., Kluzek, E., Lawrence, P. J., Li, F., Li,  
1047 H., Lombardozzi, D., Riley, W. J., Sacks, W. J., Shi, M., Vertenstein, M., Wieder, W. R., Xu, C.,  
1048 Ali, A. A., Badger, A. M., Bisht, G., Broeke, M., Brunke, M. A., Burns, S. P., Buzan, J., Clark,  
1049 M., Craig, A., Dahlin, K., Drewniak, B., Fisher, J. B., Flanner, M., Fox, A. M., Gentine, P.,  
1050 Hoffman, F., Keppel-Aleks, G., Knox, R., Kumar, S., Lenaerts, J., Leung, L. R., Lipscomb, W.  
1051 H., Lu, Y., Pandey, A., Pelletier, J. D., Perket, J., Randerson, J. T., Ricciuto, D. M., Sanderson,  
1052 B. M., Slater, A., Subin, Z. M., Tang, J., Thomas, R. Q., Martin, M. V., and Zeng, X.: The  
1053 Community Land Model Version 5: Description of New Features, Benchmarking, and Impact of  
1054 Forcing Uncertainty, *J Adv Model Earth Sy*, 11, 4245–4287,  
1055 <https://doi.org/10.1029/2018ms001583>, 2019.

1056 Leung, L. R., Bader, D. C., Taylor, M. A., and McCoy, R. B.: An Introduction to the E3SM  
1057 Special Collection: Goals, Science Drivers, Development, and Analysis, *J Adv Model Earth Sy*,  
1058 12, <https://doi.org/10.1029/2019ms001821>, 2020.

1059 Li, L., Yang, Z., Matheny, A. M., Zheng, H., Swenson, S. C., Lawrence, D. M., Barlage, M.,  
1060 Yan, B., McDowell, N. G., and Leung, L. R.: Representation of Plant Hydraulics in the Noah-  
1061 MP Land Surface Model: Model Development and Multiscale Evaluation, *J Adv Model Earth*  
1062 *Sy*, 13, <https://doi.org/10.1029/2020ms002214>, 2021.

1063 Li, Y., Li, M., Li, C., and Liu, Z.: Forest aboveground biomass estimation using Landsat 8 and  
1064 Sentinel-1A data with machine learning algorithms, *Sci Rep-uk*, 10, 9952,  
1065 <https://doi.org/10.1038/s41598-020-67024-3>, 2020.

1066 Liu, S. and Ng, G.-H. C.: A data-conditioned stochastic parameterization of temporal plant trait  
1067 variability in an ecohydrological model and the potential for plasticity, *Agr Forest Meteorol*, 274,  
1068 184–194, <https://doi.org/10.1016/j.agrformet.2019.05.005>, 2019.

1069 Longo, M., Knox, R. G., Medvigy, D. M., Levine, N. M., Dietze, M. C., Kim, Y., Swann, A. L.  
1070 S., Zhang, K., Rollinson, C. R., Bras, R. L., Wofsy, S. C., and Moorcroft, P. R.: The biophysics,  
1071 ecology, and biogeochemistry of functionally diverse, vertically and horizontally heterogeneous  
1072 ecosystems: the Ecosystem Demography model, version 2.2 – Part 1: Model description, *Geosci*  
1073 *Model Dev*, 12, 4309–4346, <https://doi.org/10.5194/gmd-12-4309-2019>, 2019.

1074 Longo, M., Saatchi, S., Keller, M., Bowman, K., Ferraz, A., Moorcroft, P. R., Morton, D. C.,  
1075 Bonal, D., Brando, P., Burban, B., Derroire, G., dos-Santos, M. N., Meyer, V., Saleska, S.,  
1076 Trumbore, S., and Vincent, G.: Impacts of Degradation on Water, Energy, and Carbon Cycling  
1077 of the Amazon Tropical Forests, *J Geophys Res Biogeosciences*, 125, e2020JG005677,  
1078 <https://doi.org/10.1029/2020jg005677>, 2020.

1079 Lu, X., Wang, Y., Wright, I. J., Reich, P. B., Shi, Z., and Dai, Y.: Incorporation of plant traits in  
1080 a land surface model helps explain the global biogeographical distribution of major forest  
1081 functional types, *Global Ecol Biogeogr*, 26, 304–317, <https://doi.org/10.1111/geb.12535>, 2017.

1082 Lundberg, S. and Lee, S.-I.: A Unified Approach to Interpreting Model Predictions, *Arxiv*, 2017.



- 1083 Lundberg, S. M., Nair, B., Vavilala, M. S., Horibe, M., Eisses, M. J., Adams, T., Liston, D. E.,  
 1084 Low, D. K.-W., Newman, S.-F., Kim, J., and Lee, S.-I.: Explainable machine-learning  
 1085 predictions for the prevention of hypoxaemia during surgery, *Nat Biomed Eng*, 2, 749–760,  
 1086 <https://doi.org/10.1038/s41551-018-0304-0>, 2018.
- 1087 Lundberg, S. M., Erion, G., Chen, H., DeGrave, A., Prutkin, J. M., Nair, B., Katz, R.,  
 1088 Himmelfarb, J., Bansal, N., and Lee, S.-I.: From local explanations to global understanding with  
 1089 explainable AI for trees, *Nat Mach Intell*, 2, 56–67, <https://doi.org/10.1038/s42256-019-0138-9>,  
 1090 2020.
- 1091 Ma, L., Hurtt, G., Ott, L., Sahajpal, R., Fisk, J., Lamb, R., Tang, H., Flanagan, S., Chini, L.,  
 1092 Chatterjee, A., and Sullivan, J.: Global Evaluation of the Ecosystem Demography Model (ED  
 1093 v3.0), *Geoscientific Model Dev Discuss*, 2021, 1–41, <https://doi.org/10.5194/gmd-2021-292>,  
 1094 2021.
- 1095 Maréchaux, I. and Chave, J.: An individual-based forest model to jointly simulate carbon and  
 1096 tree diversity in Amazonia: description and applications, *Ecol Monogr*, 87, 632–664,  
 1097 <https://doi.org/10.1002/ecm.1271>, 2017.
- 1098 Mason, N. W. H., Richardson, S. J., Peltzer, D. A., Bello, F. de, Wardle, D. A., and Allen, R. B.:  
 1099 Changes in coexistence mechanisms along a long-term soil chronosequence revealed by  
 1100 functional trait diversity: Functional diversity along ecological gradients, *J Ecol*, 100, 678–689,  
 1101 <https://doi.org/10.1111/j.1365-2745.2012.01965.x>, 2012.
- 1102 Mckay, M. D., Beckman, R. J., and Conover, W. J.: A Comparison of Three Methods for  
 1103 Selecting Values of Input Variables in the Analysis of Output From a Computer Code,  
 1104 *Technometrics*, 42, 55–61, <https://doi.org/10.1080/00401706.2000.10485979>, 2000.
- 1105 McDowell, N. G., Allen, C. D., Anderson-Teixeira, K., Aukema, B. H., Bond-Lamberty, B.,  
 1106 Chini, L., Clark, J. S., Dietze, M., Grossiord, C., Hanbury-Brown, A., Hurtt, G. C., Jackson, R.  
 1107 B., Johnson, D. J., Kueppers, L., Lichstein, J. W., Ogle, K., Poulter, B., Pugh, T. A. M., Seidl,  
 1108 R., Turner, M. G., Uriarte, M., Walker, A. P., and Xu, C.: Pervasive shifts in forest dynamics in a  
 1109 changing world, *Science*, 368, <https://doi.org/10.1126/science.aaz9463>, 2020.
- 1110 McDowell, N. G., Sapes, G., Pivovarov, A., Adams, H. D., Allen, C. D., Anderegg, W. R. L.,  
 1111 Arend, M., Breshears, D. D., Brodribb, T., Choat, B., Cochard, H., Cáceres, M. D., Kauwe, M.  
 1112 G. D., Grossiord, C., Hammond, W. M., Hartmann, H., Hoch, G., Kahmen, A., Klein, T.,  
 1113 Mackay, D. S., Mantova, M., Martínez-Vilalta, J., Medlyn, B. E., Mencuccini, M., Nardini, A.,  
 1114 Oliveira, R. S., Sala, A., Tissue, D. T., Torres-Ruiz, J. M., Trowbridge, A. M., Trugman, A. T.,  
 1115 Wiley, E., and Xu, C.: Mechanisms of woody-plant mortality under rising drought, CO<sub>2</sub> and  
 1116 vapour pressure deficit, *Nat Rev Earth Environ*, 3, 294–308, <https://doi.org/10.1038/s43017-022-00272-1>, 2022.
- 1118 McMahon, S. M., Harrison, S. P., Armbruster, W. S., Bartlein, P. J., Beale, C. M., Edwards, M.  
 1119 E., Kattge, J., Midgley, G., Morin, X., and Prentice, I. C.: Improving assessment and modelling

1120 of climate change impacts on global terrestrial biodiversity, *Trends Ecol Evol*, 26, 249–259,  
 1121 <https://doi.org/10.1016/j.tree.2011.02.012>, 2011.

1122 Medvigy, D., Wofsy, S. C., Munger, J. W., Hollinger, D. Y., and Moorcroft, P. R.: Mechanistic  
 1123 scaling of ecosystem function and dynamics in space and time: Ecosystem Demography model  
 1124 version 2, *J Geophys Res Biogeosciences* 2005 2012, 114,  
 1125 <https://doi.org/10.1029/2008jg000812>, 2009.

1126 Meng, T.-T., Wang, H., Harrison, S. P., Prentice, I. C., Ni, J., and Wang, G.: Responses of leaf  
 1127 traits to climatic gradients: adaptive variation versus compositional shifts, *Biogeosciences*, 12,  
 1128 5339–5352, <https://doi.org/10.5194/bg-12-5339-2015>, 2015.

1129 MICHALKO, R. and PEKÁR, S.: Niche partitioning and niche filtering jointly mediate the  
 1130 coexistence of three closely related spider species (Araneae, Philodromidae), *Ecol Entomol*, 40,  
 1131 22–33, <https://doi.org/10.1111/een.12149>, 2015.

1132 Mitchard, E. T. A.: The tropical forest carbon cycle and climate change, *Nature*, 559, 527–534,  
 1133 <https://doi.org/10.1038/s41586-018-0300-2>, 2018.

1134 Moorcroft, P. R.: Recent advances in ecosystem-atmosphere interactions: an ecological  
 1135 perspective, *Proc Royal Soc Lond Ser B Biological Sci*, 270, 1215–1227,  
 1136 <https://doi.org/10.1098/rspb.2002.2251>, 2003.

1137 Moorcroft, P. R., Hurtt, G. C., and Pacala, S. W.: A Method for Scaling Vegetation Dynamics:  
 1138 The Ecosystem Demography Model (ED), *Ecol Monogr*, 71, 557,  
 1139 <https://doi.org/10.2307/3100036>, 2001.

1140 Mora, C., Tittensor, D. P., Adl, S., Simpson, A. G. B., and Worm, B.: How Many Species Are  
 1141 There on Earth and in the Ocean?, *Plos Biol*, 9, e1001127,  
 1142 <https://doi.org/10.1371/journal.pbio.1001127>, 2011.

1143 Morais, T. G., Teixeira, R. F. M., Figueiredo, M., and Domingos, T.: The use of machine  
 1144 learning methods to estimate aboveground biomass of grasslands: A review, *Ecol Indic*, 130,  
 1145 108081, <https://doi.org/10.1016/j.ecolind.2021.108081>, 2021.

1146 Nearing, G. S., Kratzert, F., Sampson, A. K., Pelissier, C. S., Klotz, D., Frame, J. M., Prieto, C.,  
 1147 and Gupta, H. V.: What Role Does Hydrological Science Play in the Age of Machine Learning?,  
 1148 *Water Resour Res*, 57, <https://doi.org/10.1029/2020wr028091>, 2021.

1149 Nicotra, A. B., Atkin, O. K., Bonser, S. P., Davidson, A. M., Finnegan, E. J., Mathesius, U.,  
 1150 Poot, P., Purugganan, M. D., Richards, C. L., Valladares, F., and Kleunen, M. van: Plant  
 1151 phenotypic plasticity in a changing climate, *Trends Plant Sci*, 15, 684–692,  
 1152 <https://doi.org/10.1016/j.tplants.2010.09.008>, 2010.

1153 Oliveira, R. S., Eller, C. B., Barros, F. de V., Hirota, M., Brum, M., and Bittencourt, P.: Linking  
 1154 plant hydraulics and the fast–slow continuum to understand resilience to drought in tropical  
 1155 ecosystems, *New Phytol*, 230, 904–923, <https://doi.org/10.1111/nph.17266>, 2021.

1156 Padarian, J., McBratney, A. B., and Minasny, B.: Game theory interpretation of digital soil  
 1157 mapping convolutional neural networks, *Soil*, 6, 389–397, [https://doi.org/10.5194/soil-6-389-](https://doi.org/10.5194/soil-6-389-2020)  
 1158 [2020](https://doi.org/10.5194/soil-6-389-2020), 2020.

1159 Pal, A., Mahajan, S., and Norman, M. R.: Using Deep Neural Networks as Cost-Effective  
 1160 Surrogate Models for Super-Parameterized E3SM Radiative Transfer, *Geophys Res Lett*, 46,  
 1161 6069–6079, <https://doi.org/10.1029/2018gl081646>, 2019.

1162 Peatier, S., Sanderson, B. M., Terray, L., and Roehrig, R.: Investigating Parametric Dependence  
 1163 of Climate Feedbacks in the Atmospheric Component of CNRM-CM6-1, *Geophys Res Lett*, 49,  
 1164 <https://doi.org/10.1029/2021gl095084>, 2022.

1165 Pham, T. D., Yokoya, N., Xia, J., Ha, N. T., Le, N. N., Nguyen, T. T. T., Dao, T. H., Vu, T. T.  
 1166 P., Pham, T. D., and Takeuchi, W.: Comparison of Machine Learning Methods for Estimating  
 1167 Mangrove Above-Ground Biomass Using Multiple Source Remote Sensing Data in the Red  
 1168 River Delta Biosphere Reserve, Vietnam, *Remote Sens-basel*, 12, 1334,  
 1169 <https://doi.org/10.3390/rs12081334>, 2020.

1170 Piao, S., Wang, X., Wang, K., Li, X., Bastos, A., Canadell, J. G., Ciais, P., Friedlingstein, P., and  
 1171 Sitch, S.: Interannual variation of terrestrial carbon cycle: Issues and perspectives, *Global*  
 1172 *Change Biology*, 26, 300–318, <https://doi.org/10.1111/gcb.14884>, 2020.

1173 Poorter, L., Bongers, F., Sterck, F. J., and Wöll, H.: ARCHITECTURE OF 53 RAIN FOREST  
 1174 TREE SPECIES DIFFERING IN ADULT STATURE AND SHADE TOLERANCE, *Ecology*,  
 1175 84, 602–608, [https://doi.org/10.1890/0012-9658\(2003\)084\[0602:aorfts\]2.0.co;2](https://doi.org/10.1890/0012-9658(2003)084[0602:aorfts]2.0.co;2), 2003.

1176 Purves, D. W., Lichstein, J. W., Strigul, N., and Pacala, S. W.: Predicting and understanding  
 1177 forest dynamics using a simple tractable model, *Proc National Acad Sci*, 105, 17018–17022,  
 1178 <https://doi.org/10.1073/pnas.0807754105>, 2008.

1179 Reich, P. B.: The world-wide ‘fast–slow’ plant economics spectrum: a traits manifesto, *J Ecol*,  
 1180 102, 275–301, <https://doi.org/10.1111/1365-2745.12211>, 2014.

1181 Reichstein, M., Camps-Valls, G., Stevens, B., Jung, M., Denzler, J., Carvalhais, N., and Prabhat:  
 1182 Deep learning and process understanding for data-driven Earth system science, *Nature*, 566,  
 1183 195–204, <https://doi.org/10.1038/s41586-019-0912-1>, 2019.

1184 Rodrigues, M. and Riva, J. de la: An insight into machine-learning algorithms to model human-  
 1185 caused wildfire occurrence, *Environ Modell Softw*, 57, 192–201,  
 1186 <https://doi.org/10.1016/j.envsoft.2014.03.003>, 2014.

1187 Rouholahnejad, E., Abbaspour, K. C., Vejdani, M., Srinivasan, R., Schulin, R., and Lehmann,  
 1188 A.: A parallelization framework for calibration of hydrological models, *Environ Modell Softw*,  
 1189 31, 28–36, <https://doi.org/10.1016/j.envsoft.2011.12.001>, 2012.

1190 Sakschewski, B., Bloh, W., Boit, A., Rammig, A., Kattge, J., Poorter, L., Peñuelas, J., and  
 1191 Thonicke, K.: Leaf and stem economics spectra drive diversity of functional plant traits in a  
 1192 dynamic global vegetation model, *Global Change Biol*, 21, 2711–2725,  
 1193 <https://doi.org/10.1111/gcb.12870>, 2015.

1194 Sakschewski, B., Bloh, W. von, Boit, A., Poorter, L., Peña-Claros, M., Heinke, J., Joshi, J., and  
 1195 Thonicke, K.: Resilience of Amazon forests emerges from plant trait diversity, *Nature Climate*  
 1196 *Change*, 6, 1032–1036, <https://doi.org/10.1038/nclimate3109>, 2016.

1197 Sato, H., Itoh, A., and Kohyama, T.: SEIB–DGVM: A new Dynamic Global Vegetation Model  
 1198 using a spatially explicit individual-based approach, *Ecol Model*, 200, 279–307,  
 1199 <https://doi.org/10.1016/j.ecolmodel.2006.09.006>, 2007.

1200 Sawada, Y.: Machine Learning Accelerates Parameter Optimization and Uncertainty Assessment  
 1201 of a Land Surface Model, *J Geophys Res Atmospheres*, 125,  
 1202 <https://doi.org/10.1029/2020jd032688>, 2020.

1203 Sayad, Y. O., Mousannif, H., and Moatassime, H. A.: Predictive modeling of wildfires: A new  
 1204 dataset and machine learning approach, *Fire Safety J*, 104, 130–146,  
 1205 <https://doi.org/10.1016/j.firesaf.2019.01.006>, 2019.

1206 Shen, C.: A Transdisciplinary Review of Deep Learning Research and Its Relevance for Water  
 1207 Resources Scientists, *Water Resour Res*, 54, 8558–8593, <https://doi.org/10.1029/2018wr022643>,  
 1208 2018.

1209 Siefert, A., Violle, C., Chalmandrier, L., Albert, C. H., Taudiere, A., Fajardo, A., Aarssen, L. W.,  
 1210 Baraloto, C., Carlucci, M. B., Cianciaruso, M. V., Dantas, V. L., Bello, F., Duarte, L. D. S.,  
 1211 Fonseca, C. R., Freschet, G. T., Gaucherand, S., Gross, N., Hikosaka, K., Jackson, B., Jung, V.,  
 1212 Kamiyama, C., Katabuchi, M., Kembel, S. W., Kichenin, E., Kraft, N. J. B., Lagerström, A.,  
 1213 Bagousse-Pinguet, Y. L., Li, Y., Mason, N., Messier, J., Nakashizuka, T., Overton, J. McC.,  
 1214 Peltzer, D. A., Pérez-Ramos, I. M., Pillar, V. D., Prentice, H. C., Richardson, S., Sasaki, T.,  
 1215 Schamp, B. S., Schöb, C., Shipley, B., Sundqvist, M., Sykes, M. T., Vandewalle, M., and  
 1216 Wardle, D. A.: A global meta-analysis of the relative extent of intraspecific trait variation in  
 1217 plant communities, *Ecol Lett*, 18, 1406–1419, <https://doi.org/10.1111/ele.12508>, 2015.

1218 Sit, M., Demiray, B. Z., Xiang, Z., Ewing, G. J., Sermet, Y., and Demir, I.: A comprehensive  
 1219 review of deep learning applications in hydrology and water resources, *Water Sci Technol*, 82,  
 1220 2635–2670, <https://doi.org/10.2166/wst.2020.369>, 2020.

1221 Sitch, S., Smith, B., Prentice, I. C., Arneth, A., Bondeau, A., Cramer, W., Kaplan, J. O., Levis,  
 1222 S., Lucht, W., Sykes, M. T., Thonicke, K., and Venevsky, S.: Evaluation of ecosystem dynamics,  
 1223 plant geography and terrestrial carbon cycling in the LPJ dynamic global vegetation model: LPJ

- 1224 DYNAMIC GLOBAL VEGETATION MODEL, *Global Change Biol*, 9, 161–185,  
1225 <https://doi.org/10.1046/j.1365-2486.2003.00569.x>, 2003.
- 1226 Snell, R. S., Huth, A., Nabel, J. E. M. S., Bocedi, G., Travis, J. M. J., Gravel, D., Bugmann, H.,  
1227 Gutiérrez, A. G., Hickler, T., Higgins, S. I., Reineking, B., Scherstjanoi, M., Zurbriggen, N., and  
1228 Lischke, H.: Using dynamic vegetation models to simulate plant range shifts, *Ecography*, 37,  
1229 1184–1197, <https://doi.org/10.1111/ecog.00580>, 2014.
- 1230 Snoek, J., Larochelle, H., and Adams, R. P.: Practical Bayesian Optimization of Machine  
1231 Learning Algorithms, *Arxiv*, 2012.
- 1232 Stark, S. C., Leitold, V., Wu, J. L., Hunter, M. O., Castilho, C. V. de, Costa, F. R. C., McMahon,  
1233 S. M., Parker, G. G., Shimabukuro, M. T., Lefsky, M. A., Keller, M., Alves, L. F., Schiatti, J.,  
1234 Shimabukuro, Y. E., Brandão, D. O., Woodcock, T. K., Higuchi, N., Camargo, P. B. de,  
1235 Oliveira, R. C. de, Saleska, S. R., and Chave, J.: Amazon forest carbon dynamics predicted by  
1236 profiles of canopy leaf area and light environment, *Ecol Lett*, 15, 1406–1414,  
1237 <https://doi.org/10.1111/j.1461-0248.2012.01864.x>, 2012.
- 1238 Strigul, N., Pristinski, D., Purves, D., Dushoff, J., and Pacala, S.: SCALING FROM TREES TO  
1239 FORESTS: TRACTABLE MACROSCOPIC EQUATIONS FOR FOREST DYNAMICS, *Ecol*  
1240 *Monogr*, 78, 523–545, <https://doi.org/10.1890/08-0082.1>, 2008.
- 1241 Swenson, N. G. and Enquist, B. J.: Opposing assembly mechanisms in a Neotropical dry forest:  
1242 implications for phylogenetic and functional community ecology, *Ecology*, 90, 2161–2170,  
1243 <https://doi.org/10.1890/08-1025.1>, 2009.
- 1244 Thakur, M. P. and Wright, A. J.: Environmental Filtering, Niche Construction, and Trait  
1245 Variability: The Missing Discussion, *Trends Ecol Evol*, 32, 884–886,  
1246 <https://doi.org/10.1016/j.tree.2017.09.014>, 2017.
- 1247 Tsai, W.-P., Feng, D., Pan, M., Beck, H., Lawson, K., Yang, Y., Liu, J., and Shen, C.: From  
1248 calibration to parameter learning: Harnessing the scaling effects of big data in geoscientific  
1249 modeling, *Nat Commun*, 12, 5988, <https://doi.org/10.1038/s41467-021-26107-z>, 2021.
- 1250 Uriarte, M., Swenson, N. G., Chazdon, R. L., Comita, L. S., Kress, W. J., Erickson, D., Forero-  
1251 Montaña, J., Zimmerman, J. K., and Thompson, J.: Trait similarity, shared ancestry and the  
1252 structure of neighbourhood interactions in a subtropical wet forest: implications for community  
1253 assembly, *Ecol Lett*, 13, 1503–1514, <https://doi.org/10.1111/j.1461-0248.2010.01541.x>, 2010.
- 1254 Violle, C., Enquist, B. J., McGill, B. J., Jiang, L., Albert, C. H., Hulshof, C., Jung, V., and  
1255 Messier, J.: The return of the variance: intraspecific variability in community ecology, *Trends*  
1256 *Ecol Evol*, 27, 244–252, <https://doi.org/10.1016/j.tree.2011.11.014>, 2012.
- 1257 Wang, C., Duan, Q., Gong, W., Ye, A., Di, Z., and Miao, C.: An evaluation of adaptive surrogate  
1258 modeling based optimization with two benchmark problems, *Environ Modell Softw*, 60, 167–  
1259 179, <https://doi.org/10.1016/j.envsoft.2014.05.026>, 2014.

- 1260 Wang, S. S. -C., Qian, Y., Leung, L. R., and Zhang, Y.: Identifying Key Drivers of Wildfires in  
1261 the Contiguous US Using Machine Learning and Game Theory Interpretation, *Earth's Futur*, 9,  
1262 e2020EF001910, <https://doi.org/10.1029/2020ef001910>, 2021.
- 1263 Wang, S. S.-C., Qian, Y., Leung, L. R., and Zhang, Y.: Interpreting machine learning prediction  
1264 of fire emissions and comparison with FireMIP process-based models, *Atmos Chem Phys*, 22,  
1265 3445–3468, <https://doi.org/10.5194/acp-22-3445-2022>, 2022.
- 1266 Watson-Parris, D., Williams, A., Deaconu, L., and Stier, P.: Model calibration using ESEm  
1267 v1.1.0 – an open, scalable Earth system emulator, *Geosci Model Dev*, 14, 7659–7672,  
1268 <https://doi.org/10.5194/gmd-14-7659-2021>, 2021.
- 1269 Weng, E. S., Malyshev, S., Lichstein, J. W., Farrior, C. E., Dybzinski, R., Zhang, T.,  
1270 Shevliakova, E., and Pacala, S. W.: Scaling from individual trees to forests in an Earth system  
1271 modeling framework using a mathematically tractable model of height-structured competition,  
1272 *Biogeosciences*, 12, 2655–2694, <https://doi.org/10.5194/bg-12-2655-2015>, 2015.
- 1273 Wilson, K., Goldstein, A., Falge, E., Aubinet, M., Baldocchi, D., Berbigier, P., Bernhofer, C.,  
1274 Ceulemans, R., Dolman, H., Field, C., Grelle, A., Ibrom, A., Law, B. E., Kowalski, A., Meyers,  
1275 T., Moncrieff, J., Monson, R., Oechel, W., Tenhunen, J., Valentini, R., and Verma, S.: Energy  
1276 balance closure at FLUXNET sites, *Agr Forest Meteorol*, 113, 223–243,  
1277 [https://doi.org/10.1016/s0168-1923\(02\)00109-0](https://doi.org/10.1016/s0168-1923(02)00109-0), 2002.
- 1278 Wright, I. J., Reich, P. B., Cornelissen, J. H. C., Falster, D. S., Garnier, E., Hikosaka, K.,  
1279 Lamont, B. B., Lee, W., Oleksyn, J., Osada, N., Poorter, H., Villar, R., Warton, D. I., and  
1280 Westoby, M.: Assessing the generality of global leaf trait relationships, *New Phytol*, 166, 485–  
1281 496, <https://doi.org/10.1111/j.1469-8137.2005.01349.x>, 2005.
- 1282 Xu, T. and Liang, F.: Machine learning for hydrologic sciences: An introductory overview,  
1283 *Wiley Interdiscip Rev Water*, 8, <https://doi.org/10.1002/wat2.1533>, 2021.
- 1284 Zhang, J., Bras, R. L., Longo, M., and Scalley, T. H.: The impact of hurricane disturbances on a  
1285 tropical forest: implementing a palm plant functional type and hurricane disturbance module in  
1286 ED2-HuDi V1.0, *Geosci Model Dev*, 15, 5107–5126, [https://doi.org/10.5194/gmd-15-5107-](https://doi.org/10.5194/gmd-15-5107-2022)  
1287 [2022](https://doi.org/10.5194/gmd-15-5107-2022), 2022.
- 1288 Zhang, Y., Ma, J., Liang, S., Li, X., and Li, M.: An Evaluation of Eight Machine Learning  
1289 Regression Algorithms for Forest Aboveground Biomass Estimation from Multiple Satellite Data  
1290 Products, *Remote Sens-basel*, 12, 4015, <https://doi.org/10.3390/rs12244015>, 2020.
- 1291 Zheng, Z., Curtis, J. H., Yao, Y., Gasparik, J. T., Anantharaj, V. G., Zhao, L., West, M., and  
1292 Riemer, N.: Estimating Submicron Aerosol Mixing State at the Global Scale With Machine  
1293 Learning and Earth System Modeling, *Earth Space Sci*, 8, <https://doi.org/10.1029/2020ea001500>,  
1294 2021a.



1295 Zheng, Z., Zhao, L., and Oleson, K. W.: Large model structural uncertainty in global projections  
 1296 of urban heat waves, *Nat Commun*, 12, 3736, <https://doi.org/10.1038/s41467-021-24113-9>,  
 1297 2021b.

1298 Zheng, Z., West, M., Zhao, L., Ma, P.-L., Liu, X., and Riemer, N.: Quantifying the structural  
 1299 uncertainty of the aerosol mixing state representation in a modal model, *Atmos Chem Phys*, 21,  
 1300 17727–17741, <https://doi.org/10.5194/acp-21-17727-2021>, 2021c.

1301 Zhu, Q., Li, F., Riley, W. J., Xu, L., Zhao, L., Yuan, K., Wu, H., Gong, J., and Randerson, J.:  
 1302 Building a machine learning surrogate model for wildfire activities within a global Earth system  
 1303 model, *Geosci Model Dev*, 15, 1899–1911, <https://doi.org/10.5194/gmd-15-1899-2022>, 2022.

1304 Zuleta, D., Duque, A., Cardenas, D., Muller-Landau, H. C., and Davies, S. J.: Drought-induced  
 1305 mortality patterns and rapid biomass recovery in a terra firme forest in the Colombian Amazon,  
 1306 *Ecology*, 98, 2538–2546, <https://doi.org/10.1002/ecy.1950>, 2017.

1307